Scheme 1. Preparation of N-Substituted Polyaspartamides

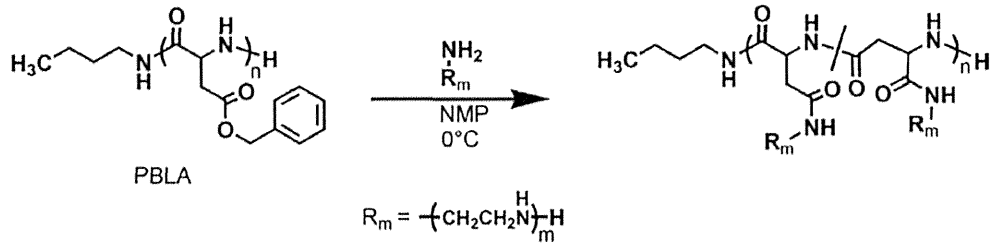

Confocal Laser Scanning Microscope (CLSM) Imaging of Polyplex Localization Inside Cells. The Label IT Cy3 Labeling Kit was used to label mRNA with Cy3 according to the manufacturer's protocol. Huh-7 cells (50 000 cells/dish) were seeded on 35 mm glass-based dishes (Iwaki, Tokyo, Japan) and were incubated overnight in 1 mL of DMEM containing 10% FBS. The medium was replaced with 1 mL of fresh medium, and 90 μL of polyplex solution containing 3 μg of Cy3-labeled mRNA (N/P = 10) was added. At 12, 24, and 48 h after transfection, the intracellular distribution of Cy3-labeled mRNA was observed using CLSM with costaining of acidic late endosomes and lysosomes using LysoTracker Green (Molecular Probes, Eugene, OR) and cell nuclei using Hoechst 33342 (Dojindo Laboratories, Kumamoto, Japan). CLSM imaging was performed using a LSM 510 instrument (Carl Zeiss, Oberlochen, Germany) with a 63× objective (C-Apochromat, Carl Zeiss, Germany) at excitation wavelengths of 488 nm for LysoTracker Green, 543 nm for Cy3, and 710 nm (MaiTai laser for 2-photon imaging) for Hoechst 33342.

Colocalization ratios of Cy3-labeled mRNA with late endosomes and lysosomes were calculated as follows:

$$\text{colocalization ratio} = \text{Cy3 pixels}_{\text{colocalization}}/\text{Cy3 pixels}_{\text{total}}$$

where Cy3 $\text{pixels}_{\text{colocalization}}$ represents the number of Cy3 pixels overlapping with LysoTracker Green, and Cy3 $\text{pixels}_{\text{total}}$ represents the total number of Cy3-positive pixels in the cell. For each condition, colocalization ratios were calculated from 10 individual cells, and the data are presented as mean ± standard error of the mean.

Hemolysis Assay. Murine erythrocytes were collected in heparin solution (10 000 units/mL) and were centrifuged at 600*g* for 5 min. The pellet was washed several times with PBS by centrifugation at 600*g* for 10 min, and finally resuspended in 1 mL of 20 mM HEPES (pH 7.4), 20 mM MES (pH 5.5), or 20 mM MES (pH 5.0) buffers containing 130 mM NaCl. PAsp(EDA), PAsp(DET), PAsp(TET), PAsp(TEP), and ExGen 500 polymer solutions were added to erythrocyte solutions at a residual amino group concentration of 5 mM, and were incubated in a shaking container at 37 °C for 30 min. After centrifugation (600*g* for 5 min), liberated hemoglobin levels were determined using colorimetric analyses of supernatants at 575 nm with a NanoDrop instrument (ND-1000 spectrophotometer, NanoDrop Technologies Inc., Wilmington, DE). To determine values for 100% hemolysis, erythrocyte solutions were lysed with 0.2 wt % Tween20. Data are presented as mean ± standard error of the mean from four samples.

Flow Cytometry Analysis to Measure Fluorescence Resonance Energy Transfer (FRET) in Cy3/Cy5-Labeled mRNA. Label IT Cy3 Labeling Kit and Label IT Cy5 Labeling Kit were used to simultaneously label mRNA with Cy3 and Cy5 with slight modification to the manufacturer's protocol. Huh-7 cells (40 000 cells/well) were seeded on 12-well culture plates and incubated for 24 h in DMEM containing 10% FBS (1 mL). Medium was replaced with an equal volume of fresh medium and 60 μL of polyplex solution containing 2 μg of Cy3/Cy5 double-labeled mRNA (N/P = 10) was added. After 8, 24, and 48 h incubation, the cells were washed twice with cold PBS and collected as suspension by trypsinization. The collected cells were centrifuged at 100*g* for 2 min and resuspended in PBS. The cells were sieved with a cell strainer prior to flow cytometry analysis. Fluorescence intensity of the cells was monitored and evaluated with a BD LSR II instrument (BD Biosciences, Franklin Lakes, NJ) equipped with FACSDiva software (BD Biosciences) using a 488 laser for excitation and a 660/20 nm filter. Data are presented as the mean ± standard error of the mean from three samples.

CLSM Imaging Analyses to Measure Fluorescence Resonance Energy Transfer (FRET) in Cy3/Cy5 mRNA. Huh-7 cells (50 000 cells/dish) were seeded on 35 mm glass-based dishes (Iwaki, Tokyo, Japan). Subcellular localization of polyplexes was investigated by incubating cells with Cellight Lysosome-GFP reagents for 16 h in 1 mL of DMEM containing 10% FBS. After replacement of media with fresh DMEM containing 10% FBS (1 mL), 90 μL of PAsp(DET) polyplex solution containing 3 μg of Cy3/Cy5 double-labeled mRNA (N/P = 10) was added. At 48 h after transfection, cells were washed with PBS and spectral imaging was performed using a super-resolution CLSM system (LSM 780: Carl Zeiss Co., Ltd., Oberlochen, Germany). The excitation wavelength for Cy3 and Cy5 was 561 nm, and that for GFP was 488 nm. Images were spectroscopically processed using the ZEN software (Carl Zeiss Co., Ltd., Oberlochen, Germany), and subcellular locations of polyplexes were determined according to GFP fluorescence.

Evaluation of Nuclease Resistance of mRNA in the Polyplexes Using FRET Analyses. Polyplex solutions containing Cy3/Cy5 double-labeled mRNA were incubated in MES (pH 5.5), HEPES (pH 7.2), or Tris-HCL (pH 9.0) buffer containing RNase A (50 μg/mL) for 1 h at 37 °C. Emission spectra for each polyplex were obtained using a NanoDrop ND-3300 fluorospectrometer (NanoDrop Technology) with excitation at 470 nm using a blue LED.

The FRET efficiency of each polyplex was calculated as follows:

$$\text{FRET efficiency} = \text{Cy3 (571nm) intensity/Cy5 (679nm) intensity}$$

FRET efficiency data were normalized to the differences between measurements taken at 0 and 1 h after addition of RNase A and are presented as the mean ± standard error of the mean from four samples.

Evaluation of Nuclease Resistance of mRNA Polyplexes Using Real Time Polymerase Chain Reaction (PCR). As in the previous section, polyplexes prepared from GLuc mRNA were incubated in MES (pH 5.5), HEPES (pH 7.2), or Tris-HCL (pH 9.0) buffer containing RNase A (5 μg/mL) for 1 h at 37 °C. Polyplex mRNA was collected using the RNeasy Mini Preparation Kit (Qiagen, Hilden, Germany) according to the manufacturer's protocol and reverse transcribed using the Quantitect Reverse Transcription Kit (Qiagen, Hilden, Germany). Subsequently, cDNA was quantified using real-time PCR with an ABI Prism 7500 instrument. The following primers were used to detect GLuc-specific sequences: forward, GGAGGTGCTCAAAGAGATGG and reverse, TTGAACCCAGGA-ATCTCAGG. Quantities of intact mRNA were expressed relative to that prior to incubation with RNase A.

Evaluation of Ethidium Bromide (EtBr) Intercalation into Polyplex mRNA. Polyplex solutions were mixed with EtBr (2.5 μg/mL) in MES (pH 5.5), HEPES (pH 7.2), or Tris-HCL (pH 9.0) buffer. After 1 h incubation at 37 °C, the fluorescence intensity at 590 nm was determined using a NanoDrop ND-1000 UV-meter (NanoDrop Technology) with excitation at 510 nm. Relative fluorescence was calculated as follows:

$$F = (F_{sample} - F_0)/(F_{100} - F_0)$$

where F_{sample}, F_{100}, and F_0 indicate the fluorescence intensity of the samples, free mRNA, and background, respectively.

Statistics. Significant differences between groups were identified using Student's t test and were considered significant when $p < 0.05$.

RESULTS AND DISCUSSION

Preparation and Characterization of N-Substituted Polyaspartamides. A series of N-substituted polyaspartamides bearing different number of side chain aminoethylene repeats (polycations) were synthesized by aminolysis reactions of β-benzyl groups of poly(β-benzyl-L-aspartate) (PBLA) with ethylenediamine (EDA), diethylenetriamine (DET), triethylenetetramine (TET), and tetraethylenepentamine (TEP) to produce poly[*N*-(2-aminoethyl)aspartamide] [PAsp(EDA)], poly{*N*′-[*N*-(2-aminoethyl)-2-aminoethyl]aspartamide} [PAsp(DET)], poly(*N*″-{*N*′-[*N*-(2-aminoethyl)-2-aminoethyl]-2-aminoethyl}aspartamide) [PAsp(TET)], and poly[*N*‴-(*N*″-{*N*′-[*N*-(2-aminoethyl)-2-aminoethyl]-2-aminoethyl}-2-aminoethyl)aspartamide] [PAsp(TEP)], respectively (Scheme 1).[9,10] This scheme of side chain aminolysis led to a synthesis of a series of polycations with same polymerization degrees and molecular weight distributions.

Changes in protonation of polycations between pHs corresponding to extracellular and endosomal pH (7.4 and 5.5, respectively) play a key role in endosomal escape of polyplexes because it determines the buffering capacity and cationic charge density of polycations, which affect interactions with cell membranes. Protonation of amino groups in the side chains of polycations can be estimated using potentiometric titrations from pH 1.2 to 11.5 (150 mM NaCl, 37 °C), as shown previously.[9]

Degrees of protonation (α) at pH 7.4 and 5.5, change in α from pH 7.4 to 5.5 ($\Delta\alpha$), and pK_a values for each polycation are summarized in Table 1. Protonated structures of side chains of each polycation were assumed from titrations, as illustrated in Scheme 2. Because PAsp(EDA) has a pK_{a1} of 9.0, its side chain is almost fully protonated at both pH values. In contrast, the major side chain in PAsp(DET) is monoprotonated at pH 7.4 and is diprotonated at pH 5.5, which crosses the pK_{a2} value of 6.2 between pH 7.4 and 5.5. The considerably low pK_{a2} value of PAsp(DET) is due to a strong electrostatic repulsion between two protonated amino groups in the diaminoethane unit, which hinders rotation according to the butane effect.[9] Likewise, the pK_{a3} value of PAsp(TET) is low due to intramolecular electrostatic repulsions, and eventually PAsp(TET) retains diprotonated side chains even at pH 5.5. The α (0.66) of PAsp(TET) at pH 5.5 is consistent with diprotonation of all side chains bearing $-CH_2CH_2-NH-CH_2CH_2-$ spacing. Because PAsp(TEP) has a pK_{a3} of 6.3 between pH 7.4 and 5.5, its major side chains are diprotonated at pH 7.4 and are triprotonated at pH 5.5. These pH-related changes in protonation of polycations reflect $\Delta\alpha$ values (Table 1), indicating that polycations bearing an even number of aminoethylene repeats (PA-Es), such as PAsp(DET) and PAsp(TEP), have larger $\Delta\alpha$ values and higher buffering capacity than those bearing an odd number of aminoethylene repeats (PA-Os), such as PAsp(EDA) and PAsp(TET).

Table 1. Degrees of Protonation (α) at pH 7.4 and 5.5, Changes in α from pH 7.4 to 5.5 ($\Delta\alpha$), and pK_a Values of N-Substituted Polyaspartamides

	α					
polycation	pH 7.4	pH 5.5	$\Delta\alpha$	pK_{a1}	pK_{a2}	pK_{a3}
PAsp(EDA)	0.93	0.99	0.06	9.0		
PAsp(DET)	0.51	0.82	0.31	8.9	6.2	
PAsp(TET)	0.56	0.66	0.10	9.1	7.8	4.3
PAsp(TEP)	0.49	0.68	0.19	9.0	8.2	6.3

Preparation of mRNA-Loaded Polyplexes from N-Substituted Polyaspartamides and Evaluation of Their Transfection Efficacy. Polyplexes loaded with Gaussia luciferase (GLuc) mRNA were prepared from polycations at the residual molar ratio of the polycation amino groups to mRNA phosphate groups (N/P) = 10. Hydrodynamic diameter and ζ-potential of these polyplexes are summarized in Supporting Information Table 1. All polyplexes showed similar size and ζ-potential of approximately 90 nm and 45 mV, respectively, regardless of the structure of polycations, indicating that the polyplexes possess similar physicochemical characteristics. Those polyplexes were then introduced into cultured human hepatoma cells (Huh-7). Transfection efficacy was evaluated over time by measuring the luminescence of secreted GLuc in the cell culture medium. Because GLuc has a half-life of 6 days in the medium,[13] luminescence assays accurately reflect cumulative GLuc expression over the incubation period. Until 12 h after mRNA introduction, PA-Es provided higher GLuc expression than PA-Os (Figure 1a). This is in a good accordance with our previous results obtained for pDNA transfection and can be explained by higher endosomal escape rates of PA-Es, which was due to the high buffering capacity and disruption of endosomal membranes induced by facilitated protonation, and particularly the formation of protonated side chain aminoethylene repeats with pH-drop in endosome.[9]

Unprecedentedly, 24 h after introduction of mRNA, a marked increase in GLuc expression was observed with the PA-Os polyplex PAsp(TET) (m = 3; Figure 1b), which produced the highest expression at 72 h among the four examined polyplexes. Similar increases in GLuc expression were observed after 10–12 h with the PA-O polyplex PAsp(EDA), which has fewer aminoethylene repeats (m = 1). However, the increase for PAsp(EDA) was less than that for PAsp(TET). Note that we also applied these mRNA polyplexes to mouse fibroblast-like cells (NIH3T3), and observed consistent expression profiles to Huh7, where PAsp(TET) provided a remarkable increase in expression 24 h after transfection (Supporting Information Figure 1). PAsp(TET) also had significantly lowered toxicity and higher transfection efficacy than a linear PEI-based commercial transfection reagent (ExGen 500; Figure 1b and Supporting Information Figure 2a). This observation indicates the practical significance of PAsp(TET) as a safe and efficient mRNA transfection reagent.

The increase in GLuc accumulation observed for PA-Os was inconsistent with our previous report, which showed greater endosomal escaping capability of PA-Es than PA-Os,[9] warranting further exploration of associated mechanisms. Cell viability after transfection and mRNA uptake did not differ significantly between the four polyplexes (Supporting Information Figure 2), excluding these factors from the reason for this trend. Then, we examined the translocation of mRNA from endosome to cytoplasm after transfection to estimate endosomal escaping capability of each polyplex. The intracellular distribution of Cy3-labeled mRNA loaded into the polyplexes

Scheme 2. Estimated Protonation of Side Chain Amino Groups in N-Substituted Polyaspartamides

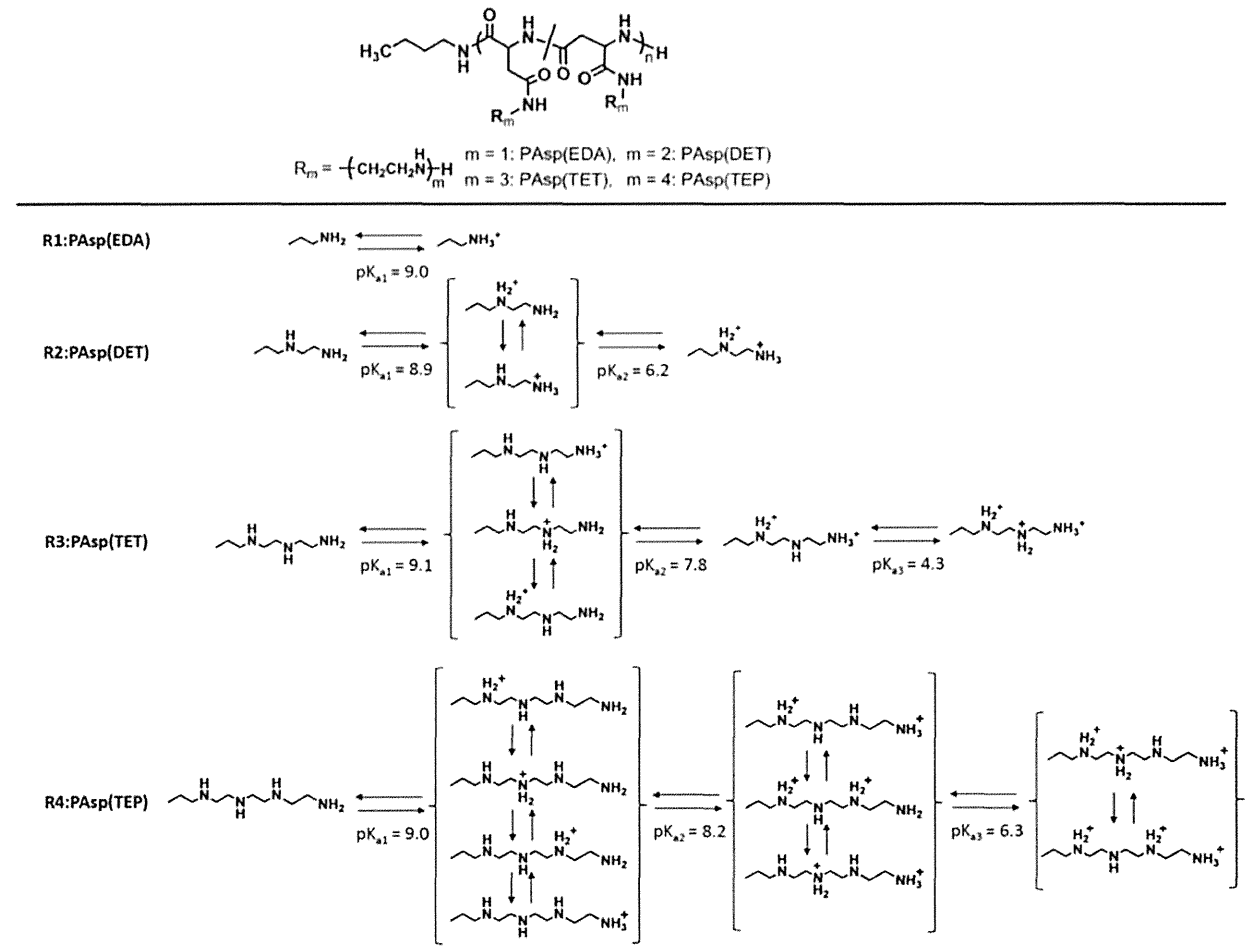

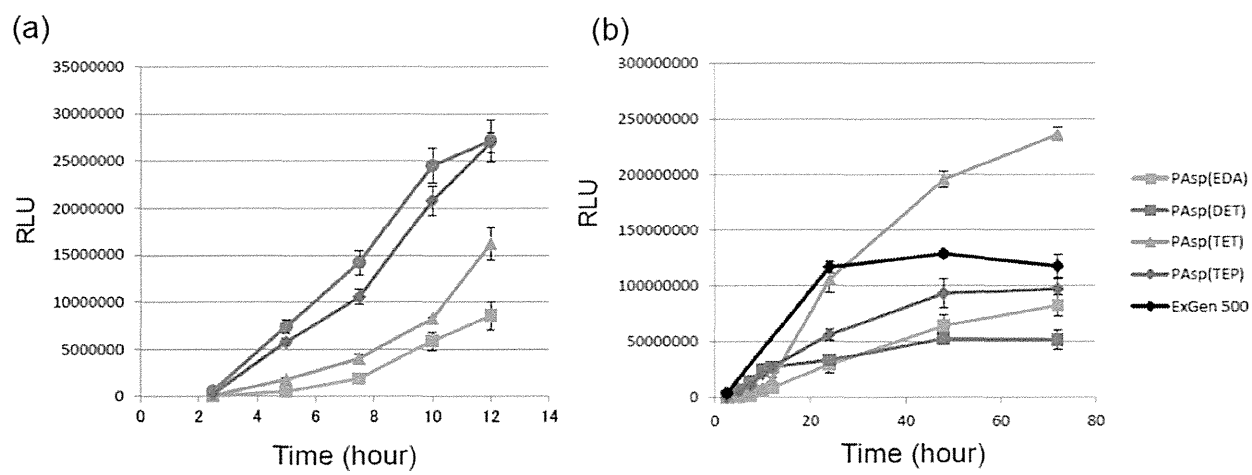

Figure 1. Cellular transfection of Gaussia luciferase (GLuc)-expressing mRNA using polyplexes prepared from N-substituted polyaspartamides. GLuc expression after transfection of mRNA polyplexes of PAsp(EDA), PAsp(DET), PAsp(TET), PAsp(TEP), or Exgen 500 into Huh-7 cells: (a) from 2 to 12 h and (b) from 2 to 72 h.

was analyzed by costaining of late endosomes and lysosomes using LysoTracker Green with a confocal laser scanning microscope (CLSM). Figure 2a–c shows typical CLSM images and indicates colocalization (yellow pixels) of Cy3-mRNA (red) with late endosomes and lysosomes (green). Colocalization ratios of the PA-Es PAsp(DET) and PAsp(TEP) were lower than those of the PA-Os PAsp(EDA) and PAsp(TET) at 12 h after transfection (Figure 2d), indicating higher capability of endosomal escape of PA-Es. This is consistent with higher Gluc expression from PA-Es than from PA-Os at 12 h (Figure

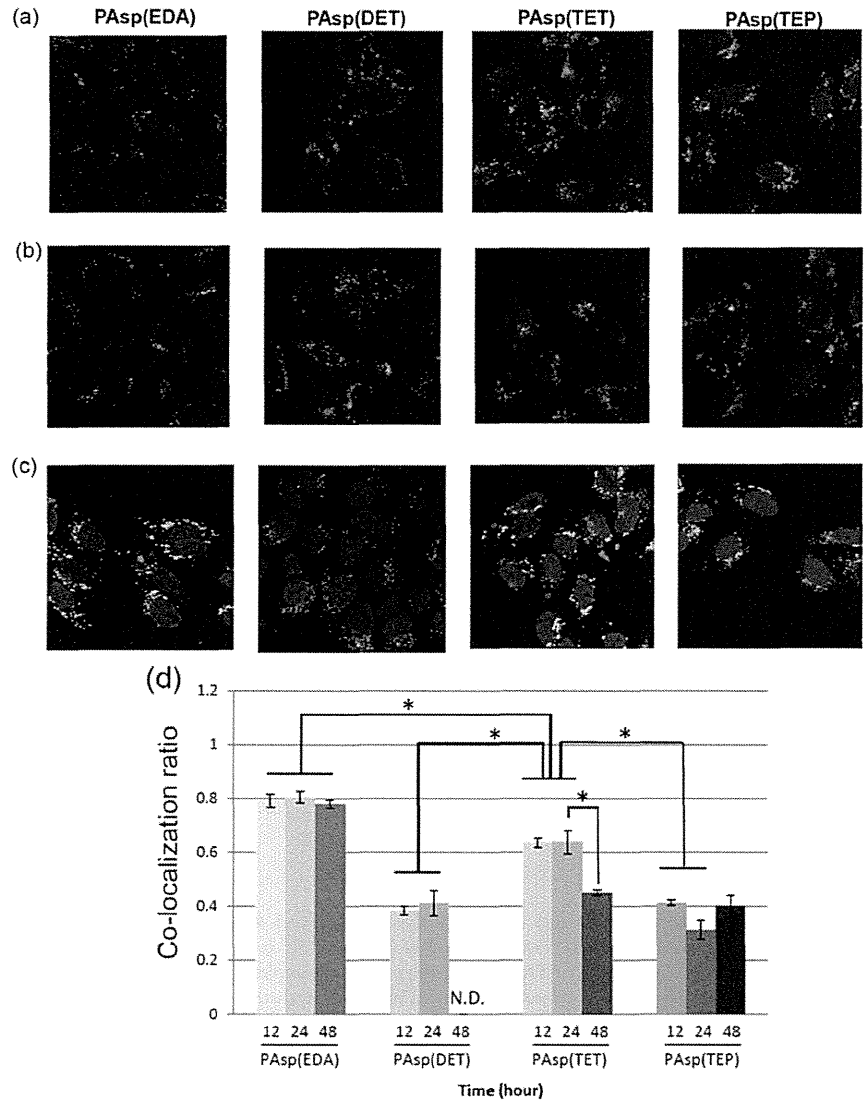

Figure 2. Colocalizatin of mRNA polyplexes with endosomes and lysosomes. Intracellular distribution of Cy3-labeled mRNA (red) polyplexes in Huh-7 cells at (a) 12, (b) 24, and (c) 48 h after transfection. Endosomes and lysosomes were stained with LysoTracker Green (green). Nuclei were stained with Hoechst 33342 (blue). (d) Colocalization ratios of Cy3-labeled mRNA with endosomes and lysosomes were calculated from fluorescent cell images taken using LSM software at 12, 24, and 48 h after transfection.

1a) and reflects acidic pH-sensitive endosomal membrane destabilization.[8,9] A significant decrease in the colocalization ratio of mRNA in late endosomes and lysosomes (green) was observed at 48 h after PAsp(TET) transfection, and this corresponded with increased GLuc expression (Figure 1b). It may be reasonable to assume that the delayed translocation of mRNA from endosomes to the cytoplasm caused the prolonged induction period of GLuc expression of PAsp(TET). As previously reported, escaping ability from acidic endosomes of polyplexes prepared form N-substituted polyaspartamides with side chain aminoethylene repeats is related to their membrane disruption activity, as evaluated from the hemolysis assays.[9] PA-Es induced significant hemolysis at pH 5.5, whereas PA-Os did not cause hemolysis under these conditions (Supporting Information Figure 3). This trend is consistent with the larger pH dependent increments of protonation ($\Delta\alpha$, pH 7.4–5.5) of the PA-Es PAsp(DET) and PAsp(TEP) compared with those of the PA-Os PAsp(EDA) and PAsp(TET), as indicated in potentiometric titrations (Table 1). However, even PAsp(TET) appeared to have hemolysis activity with further decrease in the surrounding pH from 5.5 to 5.0. Because the $\Delta\alpha$ of PAsp(TET) substantially increases between pH 5.0 and 5.5, facilitated protonation of aminoethylene repeats in the PAsp(TET) side chain may be responsible for the delayed translocation of PAsp(TET) into the cytoplasm (Supporting Information Table 2). As the drop in intravesicular pH is known to take time along the endocytic pathway from pH 6.0–6.5 in early endosomes to pH 4.5–5.5 in late endosomes and lysosomes,[14] delayed PAsp(TET)-mediated GLuc expression compared with that of PA-Es likely reflects the time course of polyplex translocation from vesicular compartments in response to decreased intravesicular pH.

PAsp(EDA), which also belongs to PA-Os, revealed similar tendencies to the PAsp(TET) system with delayed onset of GLuc expression. However, transfection efficacy was significantly lower than that for PAsp(TET), presumably because of

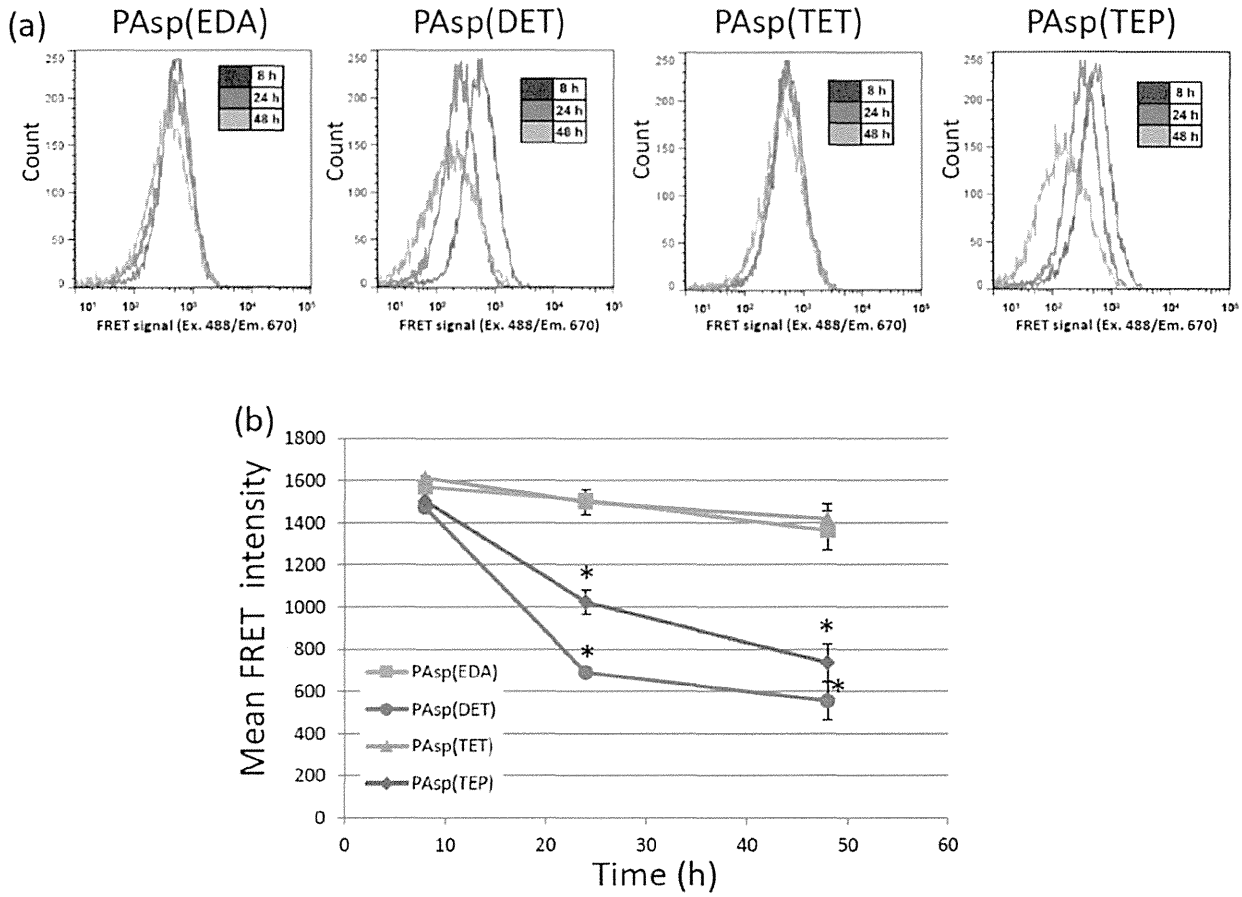

Figure 3. Intracellular fluorescence resonance energy transfer (FRET) analysis of Cy3/Cy5 double-labeled mRNA by flow cytometry after mRNA transfection. (a) Histograms of FRET signals analyzed by flow cytometry at 8, 24, and 48 h after Cy3/Cy5 double-labeled mRNA transfection of Huh-7 cells with PAsp(EDA), PAsp(DET), PAsp(TET), or PAsp(TEP) polyplex. The samples were excited with a 488 nm laser, and their emission was monitored by using a 660/20 filter. (b) Mean FRET intensity values in Huh-7 cells transfected by each polyplex were calculated at 8, 24, and 48 h from three individual experiments. Asterisk (*) indicates PA-Es showing significantly lower FRET intensity than PA-Os ($P < 0.05$).

limited endosomal escape even after 48 h (Figure 2d). This observation was consistent with our previous experiments with pDNA polyplexes, indicating that at least two protonated amino groups are required in the side chain to exert effective membrane interactions.[9]

The delayed onset in mRNA expression observed for PA-Os compared to PA-Es may be adequately explained by their slow endosomal escaping behaviors as supported by CLSM observation. However, these data do not indicate greater facilitated expression with PA-Os compared with that with PA-Es after 24 h transfection because PA-Es should have more fractions in the cytoplasm even from the early stage of transfection attributed to their superior endosomal escaping function. In this regard, it is worth noting that no mRNA was detectable in microscopy images of cytoplasmic PAsp(DET) after 48 h (Figure 2c), precluding calculation of colocalization ratios (Figure 2d). This phenomenon may reflect rapid degradation of mRNA in the cytoplasm because of instability of the polyplex. In line with this view, GLuc concentrations plateaued 24 h after transfection with the PAsp(DET) system (Figure 1b). Given the relatively long half-life of GLuc in the medium (approximately 6 days),[13] this observation indicates cessation of GLuc expression in the later time period for the PAsp(DET) system. On the other hand, continuous increases in GLuc concentrations were observed for the other three systems, indicating appreciable viability of mRNA in the cytoplasm. To get more insight in the mechanisms involved in this mRNA expression profile, we directly examined the stability of mRNA polyplexes inside cells using fluorescence resonance energy transfer (FRET).

Stability of mRNA Polyplexes in Cells: FRET Analyses of Cy3/Cy5 Double-Labeled mRNA. Because FRET efficiency should correlate with the condensation level of double-labeled mRNA, it can reflect the status of mRNA of the polyplexes in cells.[15−17] Therefore, we analyzed FRET of Cy3/Cy5 double-labeled mRNA by flow cytometry. After 8, 24, and 48 h of double-labeled mRNA transfection, FRET intensity of cells was measured by exciting the cells with a 488 nm laser and monitoring the fluorescence emission through a 660/20 nm filter. Histogram plots of FRET signal of each polycation are illustrated in Figure 3a. The histogram of PA-Es shifted more rapidly than that of PA-Os. Moreover, the mean FRET intensity of each polyplex was calculated by using FACSDiva software from individual three experiments at each time point (Figure 3b). As shown in Figure 3b, a clear odd−even effect on mean FRET intensity was observed, whereas all polyplexes showed similar cellular uptake at 24 h (Supporting Information Figure 2b). Although PA-Os maintained high FRET intensity

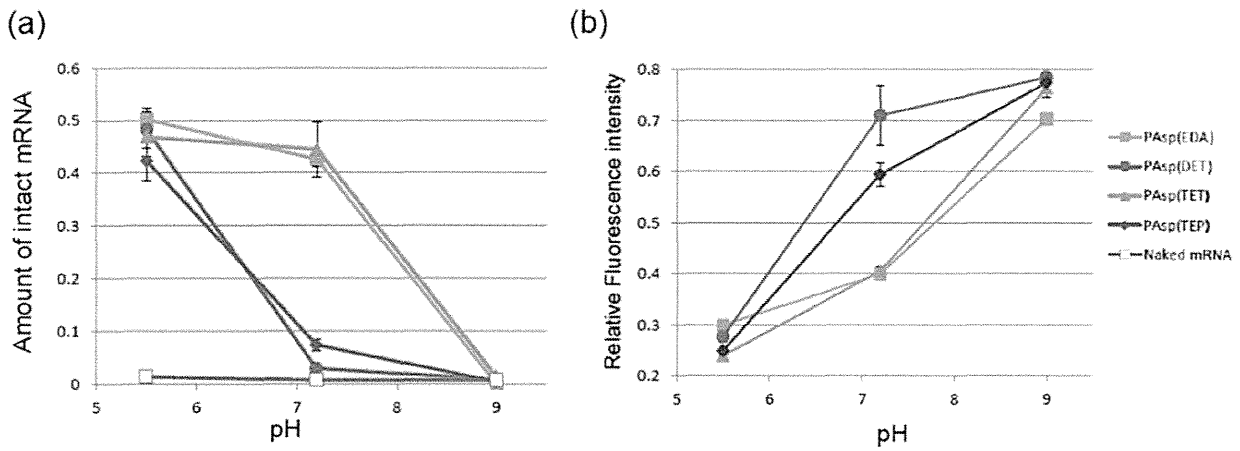

Figure 4. Evaluation of mRNA properties in the polyplexes. (a) Stability of mRNA against nuclease attack after incubation with RNase at pH 5.5, 7.2, or 9.0. (b) Ethidium bromide (EtBr) accessibility to polyplex mRNA at pH 5.5, 7.2, or 9.0.

until 48 h, FRET intensity of PA-Es decreased significantly within 24 h. This quantitative FRET analyses clearly revealed that PA-Es have lower stability in the cells and rapidly released mRNA to allow facilitated GLuc expression at the initial stage of transfection. Because the half-life of endogenous cytoplasmic mRNA in mammalian cells is estimated to several hours (median; 9 h),[18] the most plausible reason to explain the rapid decrease of PAsp(DET) FRET intensity may relate to rapid degradation of mRNA. This view is supported by the termination in GLuc production in PAsp(DET)-transfected cells after 24 h, as indicated by plateauing of GLuc accumulations (Figure 1b). In contrast, the slow and sustained escape of PA-Os from endo/lysosomal compartments and their high stability in the cells (high FRET intensities) are consistent with the observations of continuous GLuc expression. In this context, the further question was arisen from CLSM observation. At 48 h, PAsp(DET) polyplexes disappeared from cytoplasm but still remained in lysosome. To clarify this mechanism, we used a super-resolution CLSM system (LSM780, Carl Zeiss Microscopy Co., Ltd., Oberlochen, Germany) that enables analyses of Cy3 (green) and Cy5 (red) double-labeled mRNA in lysosomes costained with CellLight Lysosomes-GFP (blue; Supporting Information Figure 4). In the CLSM image, PAsp(DET) polyplexes showed the yellow pixels which reflect the colocalization of Cy3 (green) and Cy5 (red) pixels, in lysosome after 48 h transfection. This observation suggested that the mRNA in lysosome may be stably packed in PAsp(DET) polyplexes.

Enhanced Nuclease Resistance of Polyplex mRNA. To elucidate mechanisms relating to odd–even differences in stability of the polyplexes, we investigated the resistance of mRNA in the polyplexes against RNase in buffer at pH 9.0, 7.2 (cytoplasmic environment), and 5.5 (endosomal/lysosomal environment), because endonucleolytic cleavage is an important process of cytoplasmic mRNA decay.[19,20] At pH 5.5, mRNA remained intact in all the polyplexes after 1 h incubation with RNase-containing buffer (Figure 4a). In contrast, free mRNA was completely degraded, indicating substantial stability of all polyplexes under acidic conditions. This is consistent with FRET observation using CLSM (Supporting Information Figure 4) indicating a highly condensed state of mRNA in polyplexes in endosome and lysosome environments. In contrast, under nonphysiological alkaline condition (pH 9.0), mRNA in all polyplexes was completely degraded. Apparently, the protonated fraction of amino groups in the side chain dramatically decreases in alkaline condition, thereby resulting in loosening or possibly partial dissolution of the polyplex structure to allow enzyme attack toward mRNA. Indeed, the accessibility of intercalating dye, ethidium bromide (EtBr), to mRNA in the polyplexes significantly increased by changing pH from 5.5 to 9.0 as judged from an increase in relative fluorescence intensity of EtBr within mRNA (Figure 4b). Worth noting in this assay of mRNA stability against RNase is a clear difference at physiological condition (pH = 7.2) between PA-Os and PA-Es: mRNA in the PA-Es PAsp(DET) and PAsp(TEP) was almost completely degraded similarly to free mRNA, whereas that in the PA-Os PAsp(EDA) and PAsp(TET) remained intact as is the case with the result obtained at pH 5.5. EtBr assays (Figure 4b) indicated that mRNA forms more condensed structures in PA-Os than in PA-Es. Moreover, FRET analysis using the doubly labeled mRNA with Cy3 and Cy5 in RNase-containing buffer also demonstrated higher FRET efficienty for PA-Os than for PA-Es at pH 7.2 (Supporting Information Figure 5), confirming greater stability of PA-Os against RNase attack.

Proposed Mechanism of mRNA Stabilization in PA-O Polyplexes. All the present polyplexes protected mRNA from RNase attack in acidic endosomal compartments (Figure 4a and Supporting Information Figure 4). Then, smooth translocation into the cytoplasm occurs for PA-Es, even from early endosomes with a pH of approximately 6.0, reflecting facilitated protonation of diaminoethane repeats to form the diprotonated diaminoethane unit ($-NH_2^+-CH_2-CH_2-NH_2^+-$) (Scheme 2). In titration experiments, ratios of PAsp(DET) and PAsp(TEP) side chains comprising fully protonated diaminoethane units ($-NH_2^+-CH_2-CH_2-NH_2^+-$) were 40% and 52%, respectively, even at pH 6.0. Alternatively, translocation into cytoplasm is slow and limited for PA-Os as judged from the colocalization data in Figure 2d. Significant drop in the colocalization ratio for the PAsp(TET) at the later time period (48 h) is consistent with the hypothesis that appreciable pH drop in the late ensosome/lysosome (pH ~ 4.5) may facilitate the escape of polyplexes into the cytoplasm with the formation of the fully protonated array of the amino groups ($-NH_2^+-CH_2-CH_2-NH_2^+-CH_2-CH_2-NH_3^+$) in the side chain. Note that the fraction of PAsp(TET) side chain with a fully

protonated structure is calculated to be 21% at pH 4.5 from the value of pK_{a3}= 4.3. Escape of PAsp(EDA) into the cytoplasm may be limited because the absence of the repetitive protonated array is expected for the structure of this polyplex.

Although all the polyplexes offered significant protection against RNase attack under acidic conditions (pH 5.5; Figure 4a), a clear odd−even effect was observed in mRNA protection at pH 7.2, with PA-Os offering far greater stability than PA-Es. Moreover, this odd−even effect on RNase stability of loaded mRNA in the polyplexes reasonably explains their distinct behavior observed in cell experiments, and certainly worth discussing the mechanisms involved in this interesting phenomenon. As can be seen in Scheme 2, side chains of each polycation take variable protonated structures depending on pH. It is thus reasonable to assume that this variation in the protonation may play a role in the stability of mRNA in polyplexes.

Here, we focus on the pH-sensitive change in the protonation of the terminal primary amino groups. They are essentially fully protonated at pH 5.5 for all the polycations (Scheme 2), and only a fraction of primary amino groups in the PA-Es PAsp(DET) and PAsp(TEP) should be nonprotonated at pH 7.2. Given the α values of PAsp(DET) and PAsp(TEP) (0.51 and 0.49, respectively) and the feasibility of side chain protonation, half and one-third of the primary amino groups may be in the nonprotonated form on PAsp(DET) and PAsp(TEP), respectively. In contrast, primary amino groups of the PA-Os PAsp(EDA) and PAsp(TET) are almost fully protonated under these conditions. These differences in protonation of terminal primary side chain amino groups correlate with the nuclease resistance of polyplexes as follows: PAsp(EDA) = PAsp(TET) > PAsp(TEP) > PAsp(DET). Although further molecular assessments are required to elucidate details of this mechanism, the cationic charge at the end of the side chain appears indispensable to the stability of polyplex structures, particularly under nuclease attack.

CONCLUSION

The present data show that endosomal escape rates and cytoplasmic stability are important trade-off parameters determining the ultimate transfection efficacy of mRNA-loaded polyplexes formed from N-substituted polyaspartamides. Sustained protein expression was achieved by polyplexes with an odd number of aminoethylene repeats (PA-Os). This reflected stability in the cytoplasm and compensated for their inferior endosome escape rates. In contrast, polyaspartamides with an even number of aminoethylene repeats (PA-Es) showed abrupt changes in protonation between external and endosomal pH conditions, producing high enodosome escape rates. However, their poor stability in cytoplasmic condition impairs their function to sustainably express coded proteins. We previously examined pDNA-loaded polyplexes from the same series of *N*-polyaspartamide derivatives evaluated in this study[9] and showed that PA-Es had greater transfection efficiency than PA-Os. Therefore, the key transfection process to determine the efficacy may differ between mRNA and pDNA delivery systems, potentially reflecting differences in the inherent stability of mRNA and pDNA polyplexes. Higher cytoplasmic stability of pDNA compared to mRNA may shift the limiting step in transfection from the cytoplasmic stability to the efficacy of endosomal escape, thereby giving an opposite odd−even effect in transfection efficacy. These findings show that the chemistry-based design with fine-tuning in the structure of polycation to construct polyplexes is indispensably important to develop mRNA and pDNA delivery systems that may have future clinical applications.

ASSOCIATED CONTENT

Supporting Information

Additional tables with hydrodynamic diameter (D_H), polydispersity index (PDI), and ζ-potential of polyplexes, and protonation degree and $\Delta\alpha$ of N-substituted polyaspartamides. Figures showing data for GLuc expression after transfection of messenger RNA, cell viability and cellular uptake assays, hemolysis assay, FRET evaluation of Cy3/Cy5 double-labeled mRNA, and FRET efficiency of each polyplex after incubation in buffers containing RNase. This material is available free of charge via the Internet at: http://pubs.acs.org.

AUTHOR INFORMATION

Corresponding Author

kataoka@bmw.t.u-tokyo.ac.jp

Notes

The authors declare no competing financial interest.

ACKNOWLEDGMENTS

This work was financially supported in part by the Center of Innovation Program from Japan Science and Technology Agency (JST), the Funding Program for World-Leading Innovation R&D on Science and Technology (FIRST) from Japan Society for the Promotion of Sciences (JSPS), JSPS KAKENHI Grant-in-Aid for Specially Promoted Research (Grant Number 25000006 (K.K.)), Grant-in-Aid for Scientific Research (B) (Grant Number 24300170 (K.I.)), Grant-in-Aid for Research Activity Start-up (Grant Number 24800016 (H.U.)), and JSPS Core-to-Core Program, A. Advanced Research Networks. We thank Katsue Morii, Asuka Miyoshi, and Sae Suzuki (The University of Tokyo) for their technical assistance.

REFERENCES

(1) Kormann, M. S.; Hasenpusch, G.; Aneja, M. K.; Nica, G.; Flemmer, A. W.; Herber-Jonat, S.; Huppmann, M.; Mays, L. E.; Illenyi, M.; Schams, A. *Nat. Biotechnol.* **2011**, *29*, 154.

(2) Tavernier, G.; Andries, O.; Demeester, J.; Sanders, N. N.; De Smedt, S. C.; Rejman, J. *J. Controlled Release* **2011**, *150*, 238.

(3) Kabanov, A.; Kabanov, V. *Bioconjugate Chem.* **1995**, *6*, 7.

(4) Kakizawa, Y.; Kataoka, K. *Adv. Drug Delivery Rev.* **2002**, *54*, 203.

(5) Pack, D. W.; Hoffman, A. S.; Pun, S.; Stayton, P. S. *Nat. Rev. Drug Discovery* **2005**, *4*, 581.

(6) Mastrobattista, E.; van der Aa, M. A.; Hennink, W. E.; Crommelin, D. J. *Nat. Rev. Drug Discovery* **2006**, *5*, 115.

(7) Green, J. J.; Langer, R.; Anderson, D. G. *Acc. Chem. Res.* **2008**, *41*, 749.

(8) Miyata, K.; Oba, M.; Nakanishi, M.; Fukushima, S.; Yamasaki, Y.; Koyama, H.; Nishiyama, N.; Kataoka, K. *J. Am. Chem. Soc.* **2008**, *130*, 16287.

(9) Uchida, H.; Miyata, K.; Oba, M.; Ishii, T.; Suma, T.; Itaka, K.; Nishiyama, N.; Kataoka, K. *J. Am. Chem. Soc.* **2011**, *133*, 15524.

(10) Suma, T.; Miyata, K.; Ishii, T.; Uchida, S.; Uchida, H.; Itaka, K.; Nishiyama, N.; Kataoka, K. *Biomaterials* **2012**, *33*, 2770.

(11) Miyata, K.; Nishiyama, N.; Kataoka, K. *Chem. Soc. Rev.* **2012**, *41*, 2562.

(12) Wattiaux, R.; Laurent, N.; Wattiaux-De Coninck, S.; Jadot, M. *Adv. Drug Delivery Rev.* **2000**, *41*, 201.

(13) Wurdinger, T.; Badr, C.; Pike, L.; de Kleine, R.; Weissleder, R.; Breakefield, X. O.; Tannous, B. A. *Nat. Methods* **2008**, *5*, 171.

(14) Sorkin, A.; von Zastrow, M. *Nat. Rev. Mol. Cell Biol.* **2002**, *3*, 600.
(15) Itaka, K.; Harada, A.; Nakamura, K.; Kawaguchi, H.; Kataoka, K. *Biomacromolecules* **2002**, *3*, 841.
(16) Itaka, K.; Harada, A.; Yamasaki, Y.; Nakamura, K.; Kawaguchi, H.; Kataoka, K. *J. Gene Med.* **2004**, *6*, 76.
(17) Matsumoto, Y.; Itaka, K.; Yamasoba, T.; Kataoka, K. *J. Gene Med.* **2009**, *11*, 615.
(18) Schwanhäusser, B.; Busse, D.; Li, N.; Dittmar, G.; Schuchhardt, J.; Wolf, J.; Chen, W.; Selbach, M. *Nature* **2011**, *473*, 337.
(19) Schoenberg, D. R. *Wiley Interdiscip. Rev.: RNA* **2011**, *2*, 582.
(20) Schoenberg, D. R.; Maquat, L. E. *Nat. Rev. Genet.* **2012**, *13*, 246.

Biomaterials 35 (2014) 7887–7895

Contents lists available at ScienceDirect

Biomaterials

journal homepage: www.elsevier.com/locate/biomaterials

Actively-targeted polyion complex micelles stabilized by cholesterol and disulfide cross-linking for systemic delivery of siRNA to solid tumors

Yusuke Oe [a], R. James Christie [a], Mitsuru Naito [b], Stewart A. Low [b], Shigeto Fukushima [b], Kazuko Toh [a], Yutaka Miura [a], Yu Matsumoto [a], Nobuhiro Nishiyama [a, c], Kanjiro Miyata [a, **], Kazunori Kataoka [a, b, d, e, *]

[a] Center for Disease Biology and Integrative Medicine, Graduate School of Medicine, The University of Tokyo, 7-3-1 Hongo, Bunkyo-ku, Tokyo 113-0033, Japan
[b] Department of Materials Engineering, Graduate School of Engineering, The University of Tokyo, 7-3-1 Hongo, Bunkyo-ku, Tokyo 113-8656, Japan
[c] Polymer Chemistry Division, Chemical Resources Laboratory, Tokyo Institute of Technology, R1-11, 4259 Nagatsuta, Midori-ku, Yokohama 226-8503, Japan
[d] Department of Bioengineering, Graduate School of Engineering, The University of Tokyo, 7-3-1 Hongo, Bunkyo-ku, Tokyo 113-8656, Japan
[e] Center for NanoBio Integration, The University of Tokyo, 7-3-1 Hongo, Bunkyo-ku, Tokyo 113-8656, Japan

ARTICLE INFO

Article history:
Received 13 May 2014
Accepted 16 May 2014
Available online 13 June 2014

Keywords:
siRNA delivery
Polyion complex micelle
Active targeting
Cyclic RGD peptide
Cholesterol modified siRNA

ABSTRACT

For small interfering RNA (siRNA)-based cancer therapies, we report an actively-targeted and stabilized polyion complex micelle designed to improve tumor accumulation and cancer cell uptake of siRNA following systemic administration. Improvement in micelle stability was achieved using two stabilization mechanisms; covalent disulfide cross-linking and non-covalent hydrophobic interactions. The polymer component was designed to provide disulfide cross-linking and cancer cell-targeting cyclic RGD peptide ligands, while cholesterol-modified siRNA (Chol-siRNA) provided additional hydrophobic stabilization to the micelle structure. Dynamic light scattering confirmed formation of nano-sized disulfide cross-linked micelles (<50 nm in diameter) with a narrow size distribution. Improved stability of Chol-siRNA-loaded micelles (Chol-siRNA micelles) was demonstrated by resistance to both the dilution in serum-containing medium and counter polyion exchange with dextran sulfate, compared to control micelles prepared with Chol-free siRNA (Chol-free micelles). Improved stability resulted in prolonged blood circulation time of Chol-siRNA micelles compared to Chol-free micelles. Furthermore, introduction of cRGD ligands onto Chol-siRNA micelles significantly facilitated accumulation of siRNA in a subcutaneous cervical cancer model following systemic administration. Ultimately, systemically administered cRGD/Chol-siRNA micelles exhibited significant gene silencing activity in the tumor, presumably due to their active targeting ability combined with the enhanced stability through both hydrophobic interactions of cholesterol and disulfide cross-linking.

1. Introduction

Small interfering RNA (siRNA) inhibits expression of genes by a sequence-specific gene silencing effect, known as RNA interference (RNAi) [1–3]. This property has generated much interest for development of siRNA drugs that inhibit production of proteins associated with disease. However, low bioavailability of siRNA has hampered its translation into clinical use. Efforts to improve the efficacy of siRNA drugs have led to development of many types of siRNA-loaded nanoparticles to overcome biological hurdles associated with siRNA delivery, e.g., enzymatic degradation, accumulation in non-target organs/tissues and inefficient cellular uptake [4–6]. In particular, the ability to target specific cells has proven to be highly effective for enhanced accumulation of nanoparticles in solid tumors through systemic administration and has also been

* Corresponding author. Center for Disease Biology and Integrative Medicine, Graduate School of Medicine, The University of Tokyo, 7-3-1 Hongo, Bunkyo-ku, Tokyo 113-0033, Japan. Tel.: +81 3 5841 7138; fax: +81 3 5841 7139.
** Corresponding author. Tel.: +81 3 5841 1701; fax: +81 3 5841 7139.
E-mail addresses: miyata@bmw.t.u-tokyo.ac.jp (K. Miyata), kataoka@bmw.t.u-tokyo.ac.jp (K. Kataoka).

http://dx.doi.org/10.1016/j.biomaterials.2014.05.041
0142-9612/

shown to facilitate cellular/subcellular delivery of siRNA [7–16]. Thus, a variety of ligand molecules that bind to specific receptors on cancer cells have been installed on the surface of nanoparticles [7–16]. In order to take full advantage of such targeting ligands, however, maintaining the nanoparticle structure in circulation is essential; targeting ligands can cooperatively function when distributed on the nanoparticle surface, allowing for avidity through multisite binding [13,15,17,18]. Therefore, a highly effective siRNA delivery system should result from incorporating cellular surface-targeting ability to a nanoparticle platform resistant to destabilization (or dissociation), thus maximizing the ligand binding effect.

A promising platform for systemic siRNA delivery into solid tumors is the polyion complex (PIC) micelle, constructed with block copolymers of poly(ethylene glycol) (PEG) and a polycation as an siRNA binding segment [13,16,19–22]. Charge neutralization between siRNA and the polycationic segment of the block copolymer in aqueous solution enables formation of PIC micelles, in which the siRNA-loaded PIC core is surrounded by a nonionic and hydrophilic PEG shell. This core–shell structure results in enhanced colloidal stability and reduced nonspecific interactions with charged biomacromolecules. To further increase micelle stability for *in vivo* delivery, several stabilizing approaches via hydrophobic interactions [16,23] or disulfide cross-links [13,24–26] have been investigated so far. Disulfide cross-links are noteworthy as they impart reversible stability to the micelle core upon cleavage (reduction) in the cell interior in response to the increased glutathione concentration, which is 100–1000 times higher than that in the cell exterior [27,28]. Reversible micelle stability is an important feature for nucleic acid delivery vehicles, since siRNA release into the cytoplasm is required to access the RNAi pathway.

Meanwhile, our previous studies revealed that siRNA micelles could be disrupted even with disulfide cross-linking in the core, leading to undesirable release of siRNA payloads [26]. These results suggest that the cross-linking within the micelle core may be highly localized, incapable of stabilizing the whole core structure. Thus, an additional stabilizing mechanism may further reinforce the cross-linked siRNA micelle structure, leading to longer blood circulation and enhanced tumor accumulation. Herein, cholesterol-conjugated siRNA (Chol-siRNA) [29] was utilized to stabilize micelle core structures in addition to disulfide cross-linking. Hydrophobized siRNAs are expected to suppress micelle disruption and subsequent leakage of siRNA due to hydrophobic associations of cholesterol groups [16,30]. Therefore, the combined use of a thiolated block copolymer and Chol-siRNA creates a stable, yet reversible, platform for improved systemic siRNA delivery.

In this work, we employed a functional block copolymer comprising PEG segment installed with cyclo-Arg-Gly-Asp (cRGD) peptide as the tumor-targeting hydrophilic block [13,16,31] and poly(L-lysine) (PLL) segment modified with dithiobispropionimidate (DTBP) as the cationic block [26]. DTBP modification was chosen for generating a single and stable side chain structure comprising an amidine and thiol functionality, making polyionic pairs/hydrogen bonds with siRNA phosphates in addition to disulfide cross-linking [26]. After examining the contribution of Chol-siRNA to micelle stability, the targeting ability of cRGD ligand was verified utilizing a luciferase-expressing cervical cancer (HeLa-Luc) cell line. Finally, the *in vivo* siRNA delivery efficacy of the actively-targeted/stabilized micelles was evaluated by luciferase gene silencing activity in the murine subcutaneous tumors after systemic administration, demonstrating strong potential for tumor-targeted systemic siRNA delivery.

2. Materials and methods

2.1. Materials

D_2O (99.9%), tetramethylsilane (TMS, 99.5%), boric acid, trizma base and Dulbecco's modified Eagle's medium (DMEM) were purchased from Sigma Aldrich (St. Louis, MO) and used without further purification. Dithiothreitol (DTT, molecular biology grade DNase and RNase free), ethylenediamine tetraacetic acid disodium salt dihydrate (EDTA, 99.5%) and ethidium bromide solution were supplied by Wako Pure Chemical Industries (Osaka, Japan). Dimethyl-3,3′-dithiobispropionimidate/2HCl (DTBP/HCl) and slide-a-lyzer dialysis cassettes (MWCO 3500 Da) were purchased from Thermo Scientific (Rockford, IL). Sterile HEPES (1 M, pH 7.3) was purchased from Amresco (Solon, OH). Agarose L03 TAKARA was purchased from Takara Bio Inc (Shiga, Japan) and used for gel electrophoresis. Cell Counting Kit 8 (CCK-8) was purchased from Dojindo Laboratories (Kumamoto, Japan). Cyclo-[RGDfK(C-$\sum$-Acp)] (cRGD) peptide was synthesized by Peptide Institute Inc. (Osaka, Japan). A series of siRNAs were synthesized by Hokkaido System Science Co., Ltd. (Hokkaido, Japan) and their sequences were as follows; (1) firefly GL3 luciferase (siLuc): 5′-CUU ACG CUG AGU ACU UCG AdTdT-3′ (sense), 5′-UCG AAG UAC UCA GCG UAA GdTdT-3′ (antisense); (2) control scramble sequence (siScr): 5′-UUC UCC GAA CGU GUC ACG UdTdT-3′ (sense), 5′-ACG UGA CAC GUU CGG AGA AdTdT-3′ (antisense). Cy5 dye and Chol moiety were introduced to the 5′-end of the antisense strand and the sense strand, respectively.

2.2. Synthesis of cyclic RGD peptide-poly(ethylene glycol)-block-poly(L-lysine) (cRGD-PEG-PLL)

cRGD-PEG-PLL and methoxy-PEG-PLL (termed PEG-PLL) block copolymers (molecular weight (MW) of PEG: 12,000 Da; degree of polymerization (DP) of PLL segment: approximately 45) were synthesized as previously described [13,19,31]. The cRGD peptide was introduced to the PEG terminus of acetal-PEG-PLL through the thiazolidine ring formation between the N-terminal cysteine of cRGD and the aldehyde group generated in acetal-PEG-PLL after incubation at acidic pH [31]. The obtained polymer (yield: 112 mg, 86%) was characterized at 22 °C by ^{1}H NMR (JEOL ECS-400, JEOL, Tokyo, Japan). The amount of cRGD conjugated to the polymer was estimated from ^{1}H NMR spectrum based on the peak intensity ratio of phenyl protons in cRGD peptide (D-Phe, δ = 7.2–7.4 ppm) to ethylene protons in PEG ($-CH_2CH_2-$, δ = 3.6–3.8 ppm) (Fig. S1). The cRGD introduction rate was calculated to be approximately 70%.

2.3. Synthesis of cyclic RGD peptide-poly(ethylene glycol)-block-poly(L-lysine modified with 1-(3-mercaptopropyl)amidine) (cRGD-PEG-PLL(MPA))

cRGD-PEG-PLL(MPA) was synthesized by introducing MPA moieties into the lysine primary amines in cRGD-PEG-PLL using DTBP, as shown in Scheme 1 [26]. Briefly, cRGD-PEG-PLL (50 mg, 0.1 mmol amines) was dissolved in 100 mM borate buffer (pH 9.0) (10 mL), followed by the addition of DTBP/HCl (69 mg, 0.2 mmol). The reaction solution was stirred at 25 °C for 45 min and then dialyzed (MWCO 3500 Da) against 10 mM PBS (pH 6.0) for 2 h and distilled water for 2 h. The dialyzed solution was lyophilized after filtration (yield: 53.9 mg, 80%). The substitution degree of MPA groups in the obtained polymer was determined from the ^{1}H NMR spectrum based on the peak intensity ratio of β, γ and δ methylene protons in PLL side chains ($-(CH_2)_3-$, δ = 1.3–1.9 ppm) to mercaptoethyl protons in MPA moieties ($HS-(CH_2)_2-$, δ = 2.7–2.9 ppm) (Fig. 1), demonstrating quantitative introduction (>97%). In a similar manner, PEG-PLL(MPA) without cRGD peptide was synthesized by the reaction of PEG-PLL with DTBP (Scheme 1). For PEG-PLL(MPA), PEG-PLL (300 mg, 0.71 mmol amines) and DTBP/HCl (439 mg, 1.4 mol) were used (yield: 299 mg, 73%). Quantitative introduction of MPA group (>99%) was also confirmed by ^{1}H NMR analysis (Fig. S2).

2.4. Polyionic complexation of block copolymers with siRNA

cRGD-PEG-PLL(MPA) (or PEG-PLL(MPA)) block copolymer was dissolved in 10 mM HEPES buffer (pH 7.4) and incubated with 100 mM DTT at 25 °C for 15 min for disulfide reduction. The reduced polymer solution was mixed with siRNA dissolved in the same buffer (15 μM siRNA) at different molar charge ratios of the block copolymer to siRNA, i.e., amidines and primary amines in the block copolymer/phosphates in siRNA. To proceed disulfide cross-linking in the PIC core, PIC solutions (10 μM siRNA) were dialyzed (MWCO 3500 Da) against 5 mM HEPES (pH 7.4) containing 0.5% (v/v) DMSO for 2 days and 5 mM HEPES (pH 7.4) for 2 days. Dialyzed PIC solutions were filtered (0.22 μm) before characterization. In a similar manner, control PICs without Chol moieties were also prepared with PEG-PLL(MPA) and siRNA. For *in vivo* experiments, micelle solutions were dispersed in 5 mM HEPES (pH 7.4) and made isotonic by addition of 1.5 M NaCl to a final concentration of 150 mM.

2.5. Static and dynamic light scattering (SLS and DLS) analyses

SLS and DLS measurements were performed with a ZetaSizer Nano ZS instrument (Malvern Instruments Ltd., Worcestershire, UK) equipped with a He–Ne laser (λ = 633 nm) as the incident beam. All measurements were made at 25 °C and a detection angle of 173°. PIC samples (10 μM siRNA, 18 μL) dispersed in 5 mM HEPES buffer (pH 7.4) were loaded into a low-volume cuvette (Zen 2112) for each analysis.

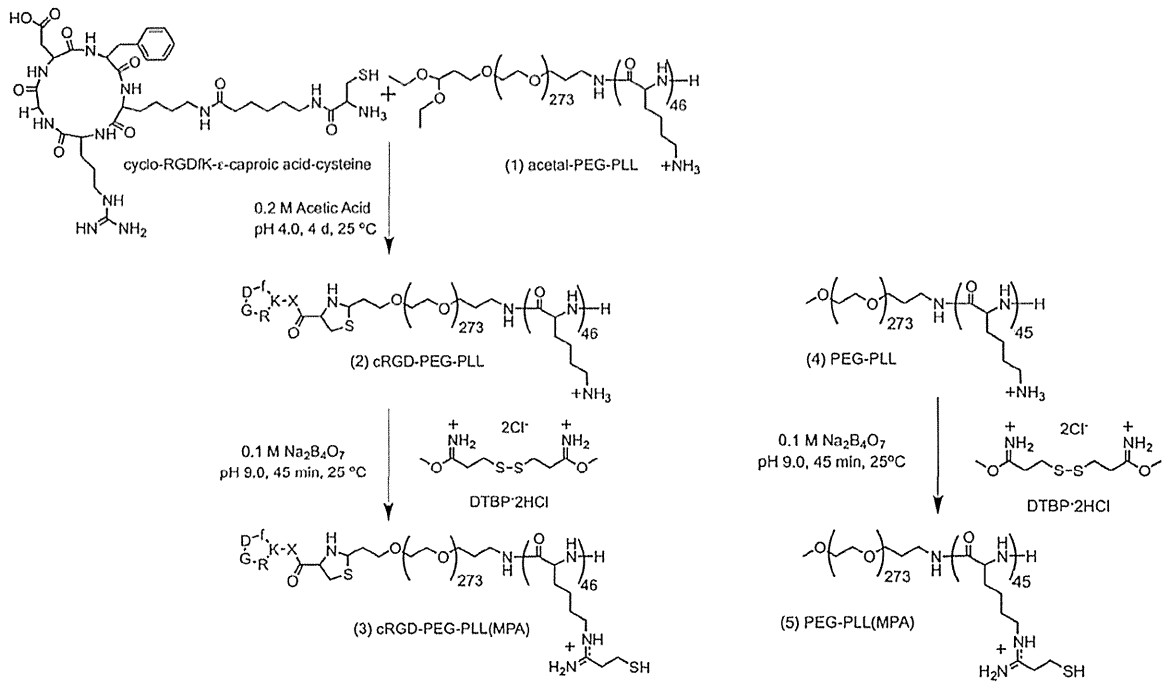

Scheme 1. Synthesis schemes of cRGD-PEG-PLL(MPA) and PEG-PLL(MPA).

Scattered light intensity (SLI) was measured to monitor micelle formation, using a constant attenuator setting in the instrument. Cumulant size, polydispersity index (PDI), and size distribution (intensity-weighted) histogram were calculated based on the autocorrelation function of samples, with automated attenuator adjustment and multiple scans (typically 12–30 scans) for optimal accuracy.

2.6. Fluorescence correlation spectroscopy (FCS) measurement

Diffusion time of fluorescently-labeled micelles (or naked siRNA) was measured by FCS using samples prepared with Cy5-labeled siRNA (Cy5-siRNA). Samples containing 10 μM Cy5-siRNA were diluted with PBS containing 10% FBS, followed by 1 h incubation. Then, the samples were placed into an 8-well Lab-Tek chambered borosilicate cover-glass (Nalge Nunc International, Rochester, NY) and measured with a combination system of ConfoCor3 module and LSM510 equipped C-Apochromat 40×, N.A. 1.2 water immersion objective (Carl Zeiss, Oberkochen, Germany) (sampling time: 10 s, repeating time: 10). A He–Ne laser (633 nm) was used for excitation of Cy5-siRNA and emission was filtered through the corresponding band-pass filter. The measured autocorrelation curves were fitted with the Zeiss Confocor3 software package to obtain the corresponding diffusion time. The obtained diffusion time was converted to the corresponding hydrodynamic diameter by the Stokes-Einstein equation.

2.7. Gel electrophoresis

Agarose gel was prepared by adding agarose (0.7 g) to a TBE buffer (70 mL) prepared with trizma base (10.8 g), boric acid (5.5 g) and EDTA/2Na (74 mg) in pure water (1 L). The mixture was heated to dissolve the agarose powder and then allowed to cool down before adding ethidium bromide (1 μL). Micelle solutions (2 μL) with or without DTT (200 mM DTT) were mixed with dextran sulfate solutions (2 μL). The concentrations of dextran sulfate groups were set at 0, 1.0, 1.5, 2.0 and 3.0 times equivalent to the siRNA phosphates. After incubation for 2 h at 25 °C, each sample was loaded on the gel and electrophoresed (100 V, 30 min) in TBE running buffer. After electrophoresis, gel images were captured by a Typhoon 9410 instrument equipped with a 532 nm laser. Also, micelle samples were subjected to the electrophoresis (50 V, 30 min) after incubation with different amounts of anionic lipid, DOPS (1,2-dioleoyl-sn-glycero-3-phospho-L-serine sodium salt), for 8 h at 25 °C.

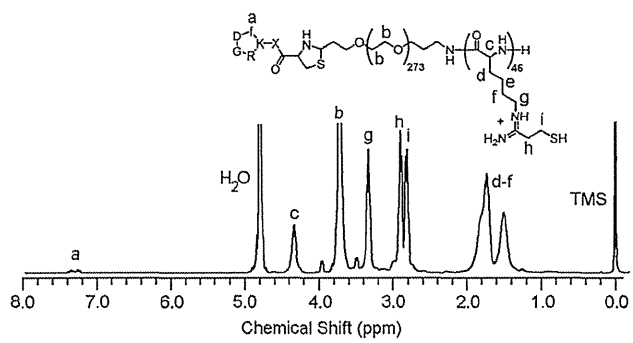

Fig. 1. ^{1}H NMR spectrum of cRGD-PEG-PLL(MPA), recorded in D_2O (10 mg/mL) at 25 °C.

2.8. Cellular uptake

Luciferase-expressing human cervical cancer cells, HeLa-Luc (Caliper LifeScience, Hopkinton, MA), were seeded into 6-well plates (100,000 cells/well) and incubated in DMEM containing 10% fetal bovine serum (FBS) (Dainippon Sumitomo Pharma Co. Osaka, Japan) (1.5 mL) for 24 h. The culture media were then exchanged with fresh media containing micelle samples prepared with Cy5-siRNA (siRNA concentration: 333 nM). Cells were incubated in the presence of micelles for 75 min at 37 °C and then further incubated in the absence of micelles for 8 h after medium exchange. The cells were harvested by trypsinization, followed by flow cytometric analyses using a BD LSR II instrument (BD Biosciences, San Jose, CA) and BD FACS Diva software (BD Biosciences).

2.9. In vitro luciferase assay

HeLa-Luc cells were seeded in 35 mm dishes (25,000 cells/dish) and incubated in DMEM containing 10% FBS (2 mL) for 24 h. Then, the culture media were exchanged with fresh media (2 mL) containing 100 μM luciferin (Summit Pharmaceutical International, Tokyo, Japan) and micelle samples (200 nM siRNA). For each analysis, control samples were prepared by treating cells with 5 mM HEPES buffer (pH 7.4). Samples were placed into a Kronos real-time photon countable incubator (ATTO Corp., Tokyo, Japan) at 37 °C and 5% CO_2 and the luminescence intensity (counts) was measured periodically over 50 h. Relative luminescence intensity was determined by normalizing the average luminescence intensity of treated samples ($n = 4$) to the average luminescence intensity of control samples ($n = 4$).

2.10. Cytotoxicity assay

HeLa-Luc cells were seeded in 24-well plates (20,000 cells/well) and incubated in DMEM containing 10% FBS (0.5 mL) for 24 h. Thereafter, the culture media were replaced with fresh media containing micelle samples at varying siRNA concentrations and cells were further incubated for 48 h. Then, CCK-8 solution (1 μL/10 μL medium) was added and samples were further incubated at 37 °C for 1 h. Cell viability was determined from the absorbance of extracellular media at 450 nm,

which was measured using a BIO-RAD 680 microplate reader (Bio-Rad, CA). All data are expressed relative to untreated control cells ($n = 6$).

2.11. Blood circulation behavior

All animal experimental procedures were performed in accordance with the policies of the Animal Ethics Committee of The University of Tokyo. The blood circulation property of siRNA-loaded micelles was determined by IVRT-CLSM observation of live mice (BALB/c nude, female, 8 weeks old) (Charles River laboratories, Tokyo, Japan) using a Nikon A1R CLSM system attached to an upright ECLIPSE FN1 (Nikon Corp., Tokyo, Japan) equipped with a 20×, 640 nm diode laser, and a band-pass emission filter of 700/75 nm, as previously described [32]. The mice were anesthetized with 2–3% isoflurane (Abbott Japan Co., Ltd., Tokyo, Japan) using a Univenter 400 anesthesia unit (Univentor Ltd., Zejtun, Malta) and placed onto the temperature-controlled microscope stage. Blood vessels in the ear-lobe dermis were observed after tail vein injection of micelles prepared with Cy5-siRNA (3.6 nmol Cy5-siRNA/mouse, $n = 3$), as they were clearly observed without surgery (thus non-invasive) and were unaffected by the cardiac beat (thus steadily observed). The obtained images were analyzed by selecting regions of interest (ROIs) within blood vessels for determining the average fluorescence intensity at each time point. To produce blood circulation profiles shown in Fig. 5A, the vein fluorescence intensities were expressed as a relative value to the highest (1.0) and the lowest (0) obtained through the observation. In addition, the time point for the highest fluorescence intensity was defined as $t = 0$.

2.12. Tumor accumulation

HeLa-Luc cells (2.6×10^6 cells) were injected under the skin of mice for preparation of donor tumors. After 2 weeks, the donor tumors were excised and cut into pieces, then transplanted under the skin of host mice. After 8 days, the subcutaneous tumor-bearing mice were subjected to tail vein injection of micelles prepared with Cy5-siRNA (1.8 nmol Cy5-siRNA/mouse, $n = 4–5$). After 4 h, they were sacrificed, and tumors (and major organs) were excised, followed by fluorescence quantification using an IVIS instrument equipped with Living Image software. Total photon counts were normalized to the illumination time and the sample area as follows: fluorescence intensity = total photons/[illumination time (s) × area (cm^2)]. Further normalization was performed by dividing the fluorescence intensity from the tumors treated with RGD-free controls.

2.13. In vivo luciferase assay

Subcutaneous HeLa-Luc tumor models were prepared by *in vivo* passage of tumor fragments, as described in the former section. After 8 days, the tumor-bearing mice were subjected to the tail vein injection of micelle samples (1.8 nmol siRNA/mouse/injection, $n = 5$) at 48 h, 38 h and 24 h before measurement. A luciferin solution (50 mM, 200 μL) was injected intraperitoneally 25 min prior to measurement to obtain the stable luminescence intensity from tumors. The luminescence intensity (counts) was recorded using an IVIS instrument under the same condition for each image (acquisition time: 5 s, binning: small, f/stop: 1, and field of view: D). Tumor volumes were determined by manual measurement with a caliper and calculated using the following equation: volume = $ab^2/2$, where a is the long axis and b is the short axis measured. The luminescence intensity obtained from sample-treated tumors was normalized to the tumor volume and further to that from buffer-treated control tumors: relative luminescence intensity = total photons of sample/sample-treated tumor volume (cm^3)/total photons of buffer control/control-treated tumor volume (cm^3).

2.14. Data analysis

The experimental data were analyzed by Student's t-test. $p < 0.05$ was considered statistically significant.

3. Results and discussion

3.1. Synthesis of block copolymers and their characterizations

In order to create actively-targeted and stabilized PIC micelles, a functional block copolymer was synthesized to comprise a targeting ligand, cationic charges, and free thiol groups (Scheme 1). The cRGD peptide was utilized as the ligand for tumor targeting through specific binding to $\alpha_v\beta_3$ and $\alpha_v\beta_5$ integrins, which are overexpressed on various cancer cells [33,34]. Also, DTBP was selected as the thiolation reagent because a cationic amidine group is concurrently introduced following reaction with lysine amines, preserving the polymer ability to form ion pairs with siRNA phosphates [26]. First, the cRGD peptide was conjugated to acetal-PEG-PLL by thiazolidine ring formation between the aldehyde generated on the PEG terminus at low pH and the N-terminal cysteine residue contained on the cRGD peptide [31]. Next, cRGD-PEG-PLL (or PEG-PLL as a non-targeted control) was reacted with DTBP under basic conditions to generate cRGD-PEG-PLL(MPA) (or PEG-PLL(MPA)) bearing the desired amidine and thiol functionalities in PLL side chains. Successful introduction of cRGD (71%) and MPA modification of amines (97%) was confirmed by ^{1}H NMR analysis of the cRGD-PEG-PLL(MPA) reaction product (Fig. 1). Similarly, quantitative reaction of DTBP with lysine amines in PEG-PLL lacking cRGD (>99%) was also confirmed (Fig. S2).

3.2. Preparation and characterization of Chol-siRNA micelles

Micelle formation behavior with Chol-siRNA was investigated in terms of SLI, size and PDI by light scattering measurements (SLS and DLS). SLI values were utilized for confirming whether i) the signal intensity (or S/N ratio) of samples was suitable for fitting and ii) the polymer/siRNA mixtures formed multimolecular assemblies (i.e. micelles) prior to fitting. The size and the PDI were then determined by appropriate fitting. PEG-PLL(MPA) was mixed with Chol-siRNA or Chol-free siRNA as a control at varying residual molar charge ratios of the block copolymer to siRNA (+:− ratio). SLI values observed for polymer/Chol-siRNA mixture increased sharply in +:− ratios from 0 to 1.2 (Fig. 2A), similar to those for Chol-free siRNA mixture, indicating formation of PIC micelles due to the charge-neutralization between the polymer and siRNA. At

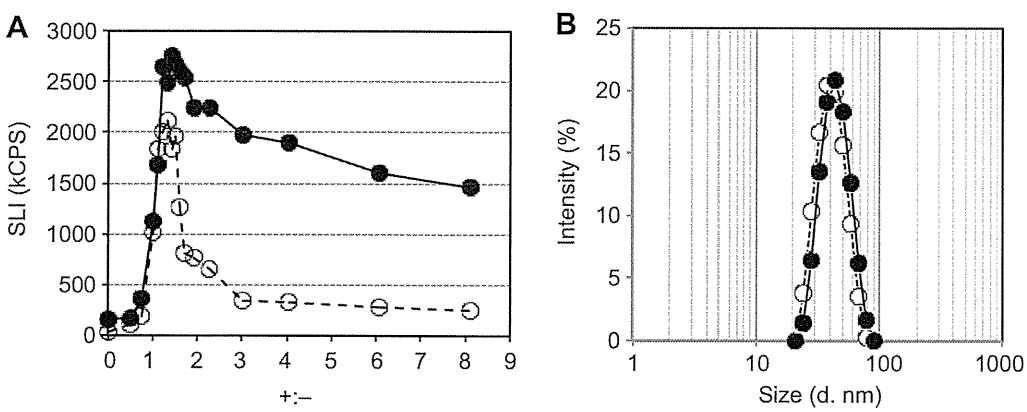

Fig. 2. Light scattering behavior of PEG-PLL(MPA) polymer and siRNA mixtures in 10 mM HEPES buffer (pH 7.4) at 25 °C. Open circles: Chol-free siRNA, closed circles: Chol-siRNA. A) SLI of mixtures at different +:− ratios. B) Intensity-weighted histograms of mixtures at +:− = 1.4.

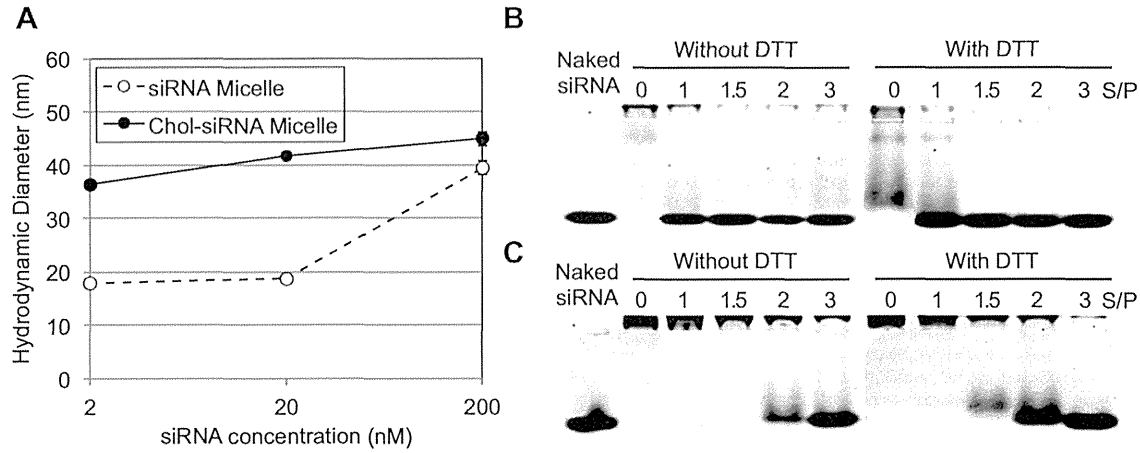

Fig. 3. Micelle stability assays. A) Change in size of Chol-free/Cy5-siRNA micelles and Chol/Cy5-siRNA micelles associated with dilution in 10% FBS-containing PBS. The diffusion time was measured by FCS and then the hydrodynamic diameter was calculated from the diffusion time (or diffusion coefficient) by the Stokes-Einstein equation. Each micelle was incubated for 1 h before measurements. Data represent the average value ± standard deviation (sampling time = 10 s, repetition time = 10). B and C) Agarose gel electrophoresis of siRNA micelles prepared with B) Chol-free siRNA and C) Chol-siRNA (0.3 μg) incubated with different concentrations of dextran sulfate under 0 or 100 mM DTT for 2 h. S/P ratio was defined as the molar ratio of sulfate groups in dextran sulfate to phosphate groups in siRNA.

+:− = 1.4, Chol-siRNA micelles were 43 ± 2 nm ($n = 3$) in cumulant diameter, and exhibited the lowest level of PDI (Fig. S3) as well as the highest SLI in the charge ratios tested. This slightly shifted +:− ratio from the charge-stoichiometric point is presumably due to the fact that complete ion-pair formation within PICs can be sterically hindered in block copolymers [26,35]. The intensity-weighted histograms at this mixing ratio clearly show the similar size distributions between Chol-siRNA and Chol-free micelles (Fig. 2B). These results confirm that the Chol moiety did not alter the micelle formation behavior between PEG-PLL(MPA) and siRNA at +:− <1.4. Note that a remarkable difference was observed between the two micelle formulations in their SLI values at +:− >1.4. The Chol-free siRNA mixture showed a drastic decrease in SLI, possibly due to the binding of a charge-excess amount of block copolymers to siRNA, generating electrostatic repulsion between PICs, and thus impeding their self-assemble into micelle structures [26]. In contrast, the Chol-siRNA mixture greatly resisted such decrease in SLI, indicating a stronger association force of Chol-siRNA PICs that can overcome electrostatic repulsion [30]. Meanwhile, the effect of MPA moieties in PEG-PLL(MPA) was additionally examined on the polyion complexation with Chol-siRNA by comparing with non-thiolated PEG-PLL. The PEG-PLL/Chol-siRNA mixtures showed the PDI of >0.18 in the tested mixing ratios from 0 to 4 (Fig. S3). These results demonstrate the crucial role of MPA moieties for the uniform micelle formation between Chol-siRNA and PEG-PLL(MPA); a possible explanation for the role of MPA moiety is that a higher degree of MPA moiety, i.e., thiol and guanidino groups, in the polycationic side chain could allow stronger intermolecular interactions with each other and/or siRNA through hydrogen bonding, dipole–dipole interactions, or Van der Waals force,

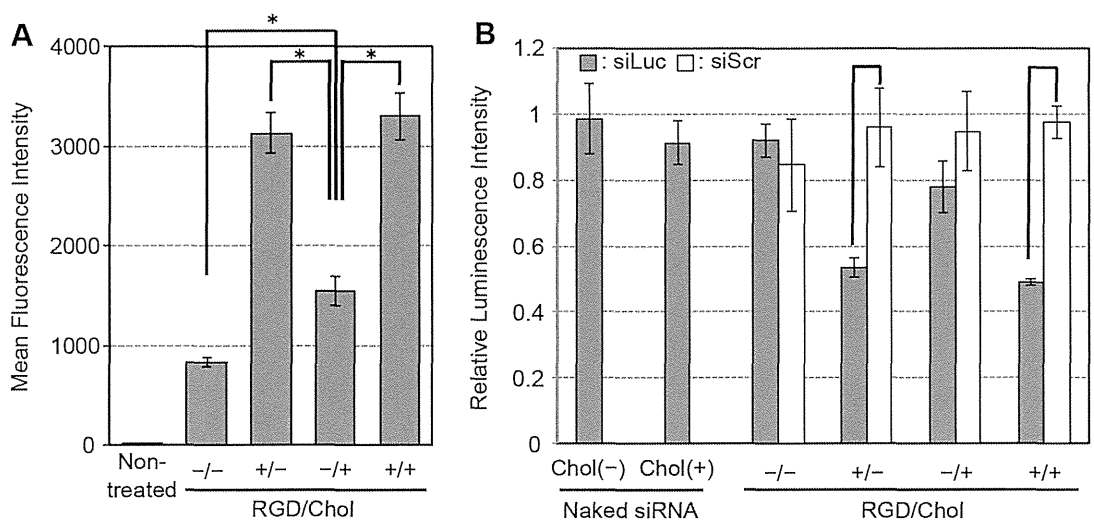

Fig. 4. A) Cellular uptake of Cy5-siRNA micelles in cultured HeLa-Luc cells, evaluated by flow cytometry. Cells were incubated with micelles for 75 min before medium change, and then further incubated for 8 h at 37 °C. Data represent the average value ± standard deviation ($n = 4$, *: $p < 0.05$). B) Gene silencing activity of naked siRNAs and siRNA micelles at 200 nM siRNA in cultured HeLa-Luc cells. Luminescence intensity was measured after 50 h incubation with siRNA samples and normalized to the value of nontreated control cells. Data represent the average value ± standard deviation ($n = 4$, *: $p < 0.05$).

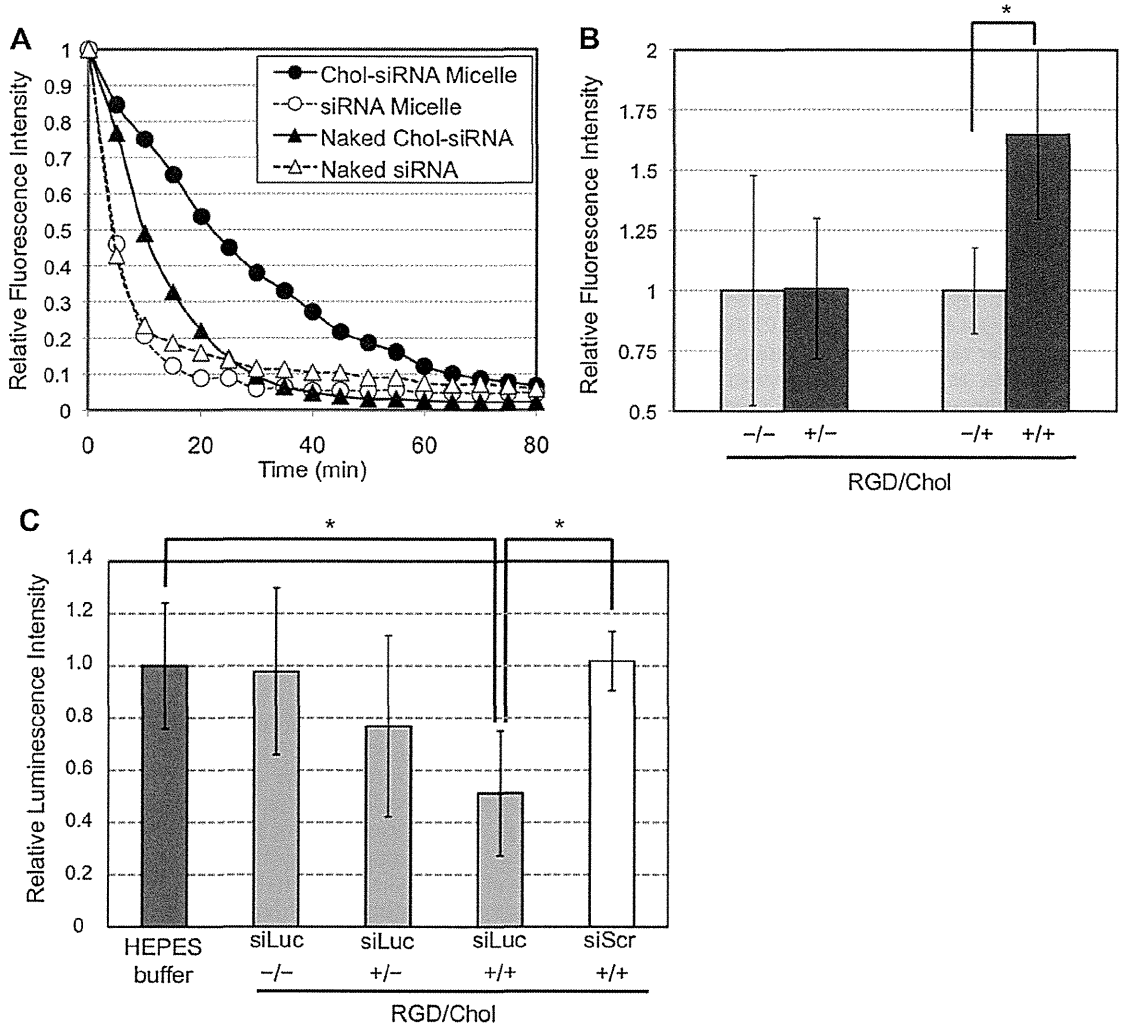

Fig. 5. *In vivo* performance of siRNA micelles. A) Blood circulation profiles, determined by IVRT-CLSM after intravenous injection (3.6 nmol siRNA/mouse) into BALB/c nude mice (open triangle: naked Chol-free/Cy5-siRNA, closed triangle: naked Chol/Cy5-siRNA, open circle: Chol-free/Cy5-siRNA micelles and closed circle: Chol/Cy5-siRNA micelles). Data represent the average value ($n = 3$). B) Relative accumulation of actively-targeted siRNA micelles to non-targeted controls in subcutaneous HeLa-Luc tumors (1.8 nmol siRNA/mouse) 4 h after intravenous injection into BALB/c nude mice. Fluorescence intensity from excised tumors was measured with an IVIS instrument, followed by the normalization as described in the Section 2.12. Data represent the average value ± standard deviation ($n = 4$ or 5, *: $p < 0.05$). C) Luciferase gene silencing activity of siRNA micelles in subcutaneous HeLa-Luc tumors. siRNA micelles were intravenously injected (1.8 nmol siRNA/mouse/injection) at 48, 38 and 24 h prior to measurement of the luminescence intensity from the excised tumors. The obtained luminescence intensity was normalized to that from the buffer-treated control tumors and the tumor volume. Data represent the average value ± standard deviation ($n = 5$, *: $p < 0.05$).

directed toward more uniform and stable micelle formation. Altogether, siRNA micelles prepared at +:− = 1.4 were used for subsequent experiments owing to the similarity in size between the two formulations as well as the sample homogeneity (lowest PDI). It should be further noted that the size distribution histograms were similar between non-targeted Chol-siRNA micelles prepared with PEG-PLL(MPA) and targeted Chol-siRNA micelles prepared with cRGD-PEG-PLL(MPA) at +:− = 1.4 (Fig. S4), suggesting that the cRGD peptide does not affect PIC formation with Chol-siRNA.

3.3. Stability of Chol-siRNA micelles

To confirm the stabilizing effect of cholesterol, the sizes of Chol-siRNA micelles and Chol-free micelles were determined under diluted conditions in 10% FBS-containing PBS by FCS measurement, which allows monitoring of the hydrodynamic size (or diffusion coefficient) of fluorescently labeled nanoparticles even in the presence of abundant serum proteins [16]. Indeed, this measurement determined the diffusion coefficients of Cy5-siRNA or Chol/Cy5-siRNA molecules complexed with the polymers, followed by conversion to hydrodynamic diameters based on the Stokes-Einstein equation (Fig. 3A). Whereas the original size of Chol-free micelles (ca. 40 nm) was maintained at 200 nM Cy5-siRNA, further dilution below 20 nM Cy5-siRNA dramatically decreased the micelle size, indicating disruption of Chol-free micelles upon dilution in the presence of FBS. It should be noted that the size of disrupted micelles (ca. 20 nm) was significantly larger than that of naked Cy5-siRNA (ca. 5 nm), suggesting that the micelles might be fragmented into small PIC fractions with a low association number of Cy5-siRNAs and block copolymers upon dilution, possibly due to limited intermolecular disulfide cross-linking within the micelle core. In contrast, Chol-siRNA micelles maintained their original size after dilution with 10% FBS, demonstrating the stabilizing effect of Chol moieties for maintaining micelle structure integrity.

Next, to further investigate micelle destabilization due to disulfide reduction as well as the stabilizing effect of Chol moieties, agarose gel electrophoresis of micelle samples was performed after incubation with or without DTT in the presence of varying concentrations of dextran sulfate (MW = 5000). This strong polyanion was used for mimicking the negatively charged extracellular matrixes, as a recent study reported that those polyanionic components play a crucial role for the destabilization of blood circulating siRNA PICs [36]. The stabilizing effect of Chol moiety was again observed upon analysis of siRNA release induced by the counter polyanions. Chol-siRNA micelles required larger amounts of dextran sulfate for the appearance of the released siRNA band, compared to Chol-free micelles (Fig. 3B and C). Futhermore, the decreased stability under the reductive conditions was confirmed for Chol-siRNA micelles, as the incubation under 100 mM DTT apparently decreased the amount of dextran sulfate required to release free siRNA from micelles (Fig. 3B and C). The similar facilitated siRNA release profiles were also observed for Chol-siRNA micelles under a cytoplasm-mimicking condition (10 mM DTT and 150 mM NaCl) in comparison with a cell exterior-mimicking condition (10 μM DTT and 150 mM NaCl) (Fig. S5A and B). Nevertheless, the modest difference between non-reductive and reductive conditions implies the significant, yet restricted contribution of disulfide cross-linking to the resistance of micelles against a strong polyanion. Note that the stabilizing effect of disulfide cross-linking was more evident under milder conditions where micelle samples were incubated with an anionic lipid molecule (DOPS). In this experiment, micelle sensitivity to reductive conditions was clearly observed even for Chol-free micelles (Fig. S5C and D).

3.4. In vitro efficacy of actively-targeted/stabilized micelles

To verify the biological effect of cRGD ligand as well as the stabilizing effect of Chol-siRNA, cellular uptake efficiencies of siRNA micelle formulations were compared by flow cytometric analyses. In this experiment, the fluorescence intensity of HeLa-Luc cells was determined after their treatment with micelles prepared with Cy5-siRNA. Note that HeLa-Luc cells were chosen as a target cell line because they overexpress integrins, especially $\alpha_v\beta_5$, on their cellular surface (Fig. S6) [31,37], and are thus appropriate for assessing the cRGD effect on cellular uptake of siRNA. Significantly higher fluorescence intensity was observed for cRGD-installed micelles, i.e., RGD(+)/Chol(−) and RGD(+)/Chol(+) micelles, in comparison with control micelles without cRGD, i.e., RGD(−)/Chol(−) and RGD(−)/Chol(+) micelles (Fig. 4A). These results highlight the effect of cRGD on the enhanced cellular uptake of siRNA micelles. In the absence of cRGD ligand, the cells incubated with RGD(−)/Chol(+) micelles showed modestly higher fluorescence intensity than those incubated with RGD(−)/Chol(−) micelles, indicating that Chol-siRNA facilitated the cellular uptake of RGD(−) micelles. Apparently, the Chol-siRNA was more effective for improving the cellular uptake of non-targeted RGD(−) micelles, compared to the targeted RGD(+) micelles. These different effects of Chol-siRNA can be explained from the standpoint of cellular uptake rate of micelles; the targeted RGD(+) micelles may be internalized more rapidly and less affected by micelle stability in cell culture conditions, compared to the non-targeted RGD(−) micelles.

Next, *in vitro* gene silencing ability of the actively-targeted/stabilized (RGD(+)/Chol(+)) micelles was evaluated by comparing with those of the other micelle formulations. siRNA for luciferase gene, i.e., siLuc, was selected for this luminescence-based gene silencing assay, which allows quantitative determination of gene silencing by comparing the luminescence intensity among samples. Fig. 4B shows the relative luminescence intensity of cells treated with each siRNA micelle (or naked siRNA) at 200 nM siRNA after 50 h incubation. The observed *in vitro* gene silencing activity is in good agreement with the results from the cellular uptake study (Fig. 4A); as cRGD-installed, RGD(+)/Chol(+) and RGD(+)/Chol(−) micelles achieved the most efficient luciferase gene silencing, followed by the RGD(−)/Chol(+) micelles and the RGD(−)/Chol(−) micelles. Actively-targeted micelles prepared with siScr induced no significant decrease in relative luminescence intensity, confirming the sequence-specific gene silencing activity of actively-targeted micelles. Consequently, the cRGD ligands installed on the micelle surface enhanced *in vitro* gene silencing activity of siRNA micelles regardless of the Chol moiety conjugated to siRNA. This is consistent with the result seen in Fig. 3A; the Chol-free micelles could avoid the rapid dissociation in the 10% serum-containing PBS under 200 nM siRNA corresponding to the transfection condition, presumably enabling ligand-mediated rapid cellular uptake. It should be noted in this regard that the Chol-free siRNA micelles prepared with cRGD-PEG-PLL without thiol (or other stabilizing) moieties induced no gene silencing under similar conditions as we reported previously [13], indicating the impact of disulfide cross-linking on gene silencing efficiency.

Cell viability following treatment with siRNA micelles was also examined in order to exclude the possibility of cytotoxic effects on the gene silencing activity of siRNA micelles. RGD(+)/Chol(−) micelles and RGD(+)/Chol(+) micelles, which showed the highest gene silencing activity, were subjected to a cell viability assay using the commercially available CCK-8 kit, based on a water soluble tetrazolium salt (WST-8). Neither micelle formulation induced significant cytotoxicity even at a high concentration of siRNA (1000 nM) (Fig. S7), indicating negligible cytotoxic effects of siRNA micelles at concentrations used for the gene silencing studies. Considering that homopolymer PLLs with a high molecular weight (e.g. 27 kDa) are known to induce significant cytotoxicity due to their cationic charges [38], this negligible cytotoxicity of the siRNA micelles might be the result that they were composed of a relatively shorter PLL segment and equipped with a PEG outer layer that masked the charged component.

3.5. In vivo efficacy of actively-targeted/stabilized micelles

Since enhanced micelle stability and active targeting ability were both demonstrated under *in vitro* conditions (Figs. 3 and 4A and B), the *in vivo* behaviors of actively-targeted/stabilized micelles were investigated following systemic administration. The longevity of siRNA micelles in the bloodstream is a critical factor for tumor accumulation of macromolecules. Prolonged circulation results in increased contact opportunity for actively-targeted micelles with the cellular surface receptors in tumor tissues.

First, the blood circulation property of fluorescently-labeled micelles (prepared with Cy5-siRNA) was evaluated by IVRT-CLSM, which can continuously monitor the fluorescence intensity of Cy5-siRNA (or its micelles) circulating in the blood of mice immediately after intravenous injection (Fig. S8A). Fluorescence intensities determined from ROIs selected within the vein were plotted against time to compare blood retention profiles of different micelle formulations (Fig. 5A). In this regard, non-targeted micelles were utilized for simply validating the effect of Chol-siRNA encapsulated within the micelles on blood retention. Chol-free micelles were rapidly eliminated from circulation, similar to naked siRNA, and consequently their blood half-life ($T_{1/2}$) was within 5 min. In sharp contrast, Chol-siRNA micelles showed significantly longer blood retention time ($T_{1/2} = >20$ min, $p < 0.05$) than Chol-free micelles. This prolonged blood circulation observed for Chol-siRNA micelles is in good agreement with the results demonstrating higher stability against dilution with serum-containing PBS (Fig. 3A) and improved resistance to polyanion

exchange with polysulfates (Fig. 3C). It is also worth mentioning that the elimination of Chol-siRNA micelles from the bloodstream followed a single exponential decay (or a one-compartment model in pharmacokinetics) (Fig. S8B), suggesting that the Chol-siRNA micelles were eliminated mainly from the kidney without being distributed into peripheral tissues. This is supported by the result that the Chol-siRNA micelles (or the siRNA payloads) were mainly accumulated in the kidney after systemic administration (Fig. S9). Note that the blood retention time of naked Chol-siRNA was modestly longer than those of naked Chol-free siRNA. This may be due to interaction of Chol-siRNA with lipoproteins in the bloodstream leading to compromised renal filtration [39].

Next, the tumor-targeting ability of cRGD-installed micelles was investigated by measuring their accumulation in subcutaneous HeLa-Luc tumors. Fluorescently-labeled micelles were administered by tail vein injection and tumors were excised after 4 h followed by measurement of the fluorescence intensity of each tumor mass with an IVIS instrument. While there was almost no difference in fluorescence intensity between Chol-free micelles with and without cRGD, significantly higher fluorescence intensity was observed for Chol-siRNA micelles equipped with cRGD, compared to those without cRGD (Fig. 5B). These results indicate that the cRGD ligand enabled more efficient tumor accumulation of the highly stabilized Chol-siRNA micelles following systemic administration, presumably due to the enhanced avidity of cRGD ligands to $\alpha_v\beta_3/\alpha_v\beta_5$ integrin receptors on cancerous cells and also tumor-associated endothelial cells [13,33,34]. Intratumoral distribution of RGD(+)/Chol(+) micelles was further examined by continuous CLSM observation of the subcutaneous tumor tissue after systemic administration. The CLSM image captured at 80 min after injection displays massive distribution of the micelles in the tumor tissue through the blood vessels (Fig. S10). Importantly, there were no significant differences in healthy organ/tissue accumulation between non-targeted and actively-targeted micelles ($p > 0.05$) (Fig. S9), demonstrating tumor-selective targeting of RGD(+)/Chol(+) micelles.

Finally, the *in vivo* gene silencing activity of siRNA micelles was investigated through luciferase gene silencing (luminescence measurement) in subcutaneous HeLa-Luc tumors, similar to the luminescence-based assay used for *in vitro* experiments. At 48 h after the initial injection of samples (total 3 intravenous injections), luciferin solution was intraperitoneally injected into mice, followed by measurement of the luminescence intensity in the tumor tissues with an IVIS instrument (Fig. 5C and Fig. S11). Non-targeted RGD(−)/Chol(−) micelles did not decrease tumor luminescence intensity, whereas the actively-targeted, RGD(+)/Chol(−) and RGD(+)/Chol(+) micelles did reduce tumor luminescence intensities compared to buffer-treated controls. In particular, the actively-targeted/stabilized, RGD(+)/Chol(+) micelles achieved significant decrease in the luminescence intensity ($p < 0.05$ for buffer-treated controls). It should be noted that the RGD(+)/Chol(+) micelles carrying siScr as a control sequence caused no decrease in the luminescence intensity, demonstrating sequence-specific gene silencing (i.e. RNAi) activity of the actively-targeted/stabilized micelles. In addition, it was also confirmed that all the tested micelles did not induce significant changes in the body weight of tumor-bearing mice (Table S1). In total, actively-targeted and stabilized micelles were more effective in delivering intact (thus active) siRNA to the cytoplasm of tumor cells following systemic administration. The present study particularly focused on the separate functionalization of the macromolecular components, i.e., PEG-PLL and siRNA, for construction of the multifunctional formulation, i.e., actively-targeted/stabilized micelles. This approach permitted the facile functionalization based on a simple chemistry, which is in contrast to the previously developed block copolymer modified with 2-iminothiolane, where two functional groups, open chain and closed ring structures, are equilibrated in the side chain of PLL [13].

4. Conclusions

Actively-targeted and stabilized PIC micelles were constructed with Chol-siRNA and PEG-PLL comprising the cRGD ligand at the PEG terminus and thiol (and amidine) functionality in PLL side chains, for systemic siRNA delivery to solid tumors. The Chol modification of siRNA allowed the production of PIC micelles at wider mixing ratios above the charge-stoichiometric point and dramatically stabilized the micelle structure, resulting in the enhanced blood circulation property of siRNA micelles. Further, the active targeting ability of the cRGD ligand was proven by enhanced cellular uptake *in vitro* and also enhanced tumor accumulation *in vivo* following systemic administration. Ultimately, the synergistic effect of active targetability and improved stability enabled significant sequence-specific gene silencing in the subcutaneous tumor tissue following systemic administration of siRNA micelles. The results obtained in this study highlight the importance of additional stabilizing mechanisms in PIC micelle systems, and that stabilization can be achieved from both the polymer component and the siRNA component used. Here, Chol-conjugation to siRNA reinforced the limited effect of disulfide cross-linking, thus improving the active targetability of nanoparticulate formulations for systemic transport of siRNA into tumor tissues.

Acknowledgments

This research was financially supported by the Funding Program for World-Leading Innovate R&D in Science and Technology (FIRST) (JSPS), Grants-in-Aid for Scientific Research of MEXT (JSPS KAKENHI Grant Numbers 25000006 and 25282141), the Center of Innovation (COI) Program (JST), Grants-in-Aid for Scientific Research of MHLW, National Institute of Biomedical Innovation and Mochida Memorial Foundation for Medical and Pharmaceutical Research.

Appendix A. Supplementary data

Supplementary data related to this article can be found online at http://dx.doi.org/10.1016/j.biomaterials.2014.05.041.

References

[1] Fire A, Xu S, Montogomery M, Kostas S, Driver S, Mello C. Potent and specific genetic interference by double stranded RNA in caenorhabditis elegans. Nature 1998;391:806–11.
[2] Elbashir SM, Harborth J, Lendeckel W, Yalcin A, Weber K, Tuschl T. Duplexes of 21-nucleotide RNAs mediate RNA interference in cultured mammalian cells. Nature 2001;411:494–8.
[3] Burnett JC, Rossi JJ. RNA-based therapeutics: current progress and future prospects. Chem Biol Rev 2012;19:60–71.
[4] Carthew R, Sontheimer E. Origins and mechanisms of miRNA and siRNAs. Cell 2009;136:642–55.
[5] Turner J, Jones S, Moschos S, Lindsay M, Gait M. MALDI-TOF mass spectral analysis of siRNA degradation in serum confirms an RNase A-like activity. Mol Biosyst 2007;3:43–50.
[6] Van de Water F, Boerman O, Wouterse A, Peters J, Russel F, Masereeuw R. Intravenously administered short interfering RNA accumulates in the kidney and selectively suppresses gene function in renal proximal tubules. Drug Metab Dispos 2006;34:1393–7.
[7] Schiffelers RM, Ansari A, Xu J, Zhou Q, Tang Q, Strom G, et al. Cancer siRNA therapy by tumor selective delivery with ligand-targeted sterically stabilized nanoparticle. Nucleic Acids Res 2004;32:e149.
[8] Song E, Zhu P, Lee SK, Chowdhury D, Kussman S, Dykxhoorn DM, et al. Antibody mediated in vivo delivery of small interfering RNAs via cell-surface receptors. Nat Biotechnol 2005;23:709–17.

[9] McNamara II JO, Andrechek ER, Wang Y, Viles KD, Rempel RE, Gilboa E, et al. Cell type-specific delivery of siRNAs with aptamer-siRNA chimeras. Nat Biotechnol 2006;24:1005–15.
[10] Li SD, Chen YC, Hackett MJ, Huang L. Tumor-targeted delivery of siRNA by self-assembled nanoparticles. Mol Ther 2008;16:163–9.
[11] Wang XL, Xu R, Wu X, Gillespie D, Jensen R, Lu ZR. Targeted systemic delivery of a therapeutic siRNA with a multifunctional carrier controls tumor proliferation in mice. Mol Pharm 2009;6:738–46.
[12] Davis ME, Zuckerman JE, Choi CHJ, Seligson D, Tolcher A, Alabi CA, et al. Evidence of RNAi in humans from systemically administered siRNA via targeted nanoparticles. Nature 2010;64:1067–70.
[13] Christie RJ, Matsumoto Y, Miyata K, Nomoto T, Fukushima S, Osada K, et al. Targeted polymeric micelles for siRNA treatment of experimental cancer by intravenous injection. ACS Nano 2012;6:5174–89.
[14] Dohmen C, Edinger D, Frohlich T, Schreiner L, Lachelt U, Troiber C, et al. Nanosized multifunctional polyplexes for receptor-mediated siRNA delivery. ACS Nano 2012;26:5198–208.
[15] Lee H, Lytton-Jean AKR, Chen Y, Love KT, Park AI, Karagiannis ED, et al. Molecularly self-assembled nucleic acid nanoparticles for targeted in vivo siRNA delivery. Nat Nanotechnol 2012;7:389–93.
[16] Kim HJ, Ishii T, Zheng M, Watanabe S, Toh K, Matsumoto Y, et al. Multifunctional polyion complex micelle featuring enhanced stability, targetability, and endosome escapability for systemic siRNA delivery to subcutaneous model of lung cancer. Drug Deliv Transl Res 2014;4:50–60.
[17] Jule E, Nagasaki Y, Kataoka K. Surface plasmon resonance study on the interaction between lactose-installed poly(ethylene glycol)-poly(D, L-lactide) block copolymer micelles and lectins immobilized on a gold surface. Langmuir 2002;18:10334–9.
[18] Alam MR, Ming X, Fisher M, Lackey JG, Rajeev KG, Manoharan M, et al. Multivalent cyclic RGD conjugates for targeted delivery of small interfering RNA. Bioconjug Chem 2011;22:1673–81.
[19] Harada A, Kataoka K. Formation of polyion complex micelles in an aqueous milieu from a pair of oppositely-charged block copolymers with poly(ethylene glycol) segments. Macromolecules 1995;28:5294–9.
[20] Kataoka K, Togawa H, Harada A, Yasugi K, Matsumoto T, Katayose S. Spontaneous formation of polyion complex micelles with narrow distribution from antisense oligonucleotide and cationic block copolymer in physiological saline. Macromolecules 1996;29:8556–7.
[21] Kakizawa Y, Kataoka K. Block copolymer micelles for delivery of gene and related compounds. Adv Drug Deliv Rev 2002;54:203–22.
[22] Miyata K, Nishiyama N, Kataoka K. Rational design of smart supramolecular assemblies for gene delivery: chemical challenges in the creation of artificial viruses. Chem Soc Rev 2012;41:2562–74.
[23] Kim HJ, Oba M, Pittella F, Nomoto T, Cabral H, Matsumoto Y, et al. PEG-detachable cationic polyaspartamide derivatives bearing stearoyl moieties for systemic siRNA delivery toward subcutaneous BxPC3 pancreatic tumor. J Drug Target 2012;20:33–42.
[24] Kakizawa Y, Harada A, Kataoka K. Environment-sensitive stabilization of core-shell structured polyion complex micelle by reversible cross-linking of the core through disulfide bond. J Am Chem Soc 1999;121:11247–8.
[25] Matsumoto S, Christie RJ, Nishiyama N, Miyata K, Ishii A, Oba M, et al. Environment-responsive block copolymer micelles with a disulfide cross-linked core for enhanced siRNA delivery. Biomacromolecules 2009;10:119–27.
[26] Christie RJ, Miyata K, Matsumoto Y, Nomoto T, Menasco D, Lai TC, et al. Effect of polymer structure on micelles formed between siRNA and cationic block copolymer comprising thiols and amidines. Biomacromolecules 2011;12:3174–85.
[27] Meister A, Anderson ME. Glutathione. Annu Rev Biochem 1983;52:711–60.
[28] Saito G, Swanson JA, Lee KD. Drug delivery strategy utilizing conjugation via reversible disulfide linkages: role and site of cellular reducing activities. Adv Drug Deliv Rev 2013;55:199–215.
[29] Soutschek J, Akinc A, Bramlage B, Charisse K, Constien R, Donoghue M, et al. Therapeutic silencing of an endogenous gene by systemic administration of modified siRNAs. Nature 2004;432:173–8.
[30] Oba M, Miyata K, Osada K, Christie RJ, Sanjoh M, Li W, et al. Polyplex micelles prepared from ω-cholesteryl PEG-polycation block copolymers for systemic gene delivery. Biomaterials 2011;32:652–63.
[31] Oba M, Fukushima S, Kanayama N, Aoyagi K, Nishiyama N, Koyama H, et al. Cyclic RGD peptide-conjugated polyplex micelles as a targetable gene delivery system directed to cells possessing αvβ3 and αvβ5 integrins. Bioconjug Chem 2007;18:1415–23.
[32] Matsumoto Y, Nomoto T, Cabral H, Mastumoto Y, Watanabe S, Christie RJ, et al. Direct and instantaneous observation of intravenously injected substances using intravital confocal micro-videography. Biomed Opt Express 2010;1:1209–16.
[33] Ruoslahti E. RGD and recognition sequences for integrins. Annu Rev Cell Dev Biol 1996;12:697–715.
[34] Xiong J, Stehle T, Zhang R, Joachimiak A, Frech M, Goodman S, et al. Crystal structure of the extra-cellular segment of integrin αvβ3 in complex with an Arg-Gly-Asp ligand. Science 2002;296:151–5.
[35] Itaka K, Yamauchi K, Harada A, Nakamura K, Kawaguchi H, Kataoka K. Polyion complex micelles from plasmid DNA and poly(ethyleneglycol)-poly(L-lysine) block copolymer as serum-tolerable polyplex system: physicochemical properties of micelles relevant to gene transfection efficiency. Biomaterials 2003;24:4495–506.
[36] Zukerman JE, Choi CHJ, Han H, Davis ME. Polycation-siRNA nanoparticles can disassemble at the kidney glomerular basement membrane. Proc Natl Acad Sci U S A 2012;109:3137–42.
[37] Shayakhmetov DM, Eberly AM, Li ZY, Lieber A. Deletion of penton RGD motifs affects the efficiency of both the internalization and the endosome escape of viral particles containing adenovirus serotype 5 or 35 fiber knobs. J Virol 2005;79:1053–61.
[38] Symonds P, Murray JC, Hunter AC, Debska G, Szewczyk A, Moghimi SM. Low and high molecular weight poly(L-lysine)s/poly(L-lysine)-DNA complexes initiate mitochondrial-mediated apoptosis differently. FEBS Lett 2005;579:6191–8.
[39] Wolfrum C, Shi S, Jayaprakash KN, Jayaraman M, Wang G, Pandey RK, et al. Mechanisms and optimization of *in vivo* delivery of lipophilic siRNAs. Nat Biotechnol 2007;25:1149–57.

Fine-Tuning of Charge-Conversion Polymer Structure for Efficient Endosomal Escape of siRNA-Loaded Calcium Phosphate Hybrid Micelles

Yoshinori Maeda, Frederico Pittella, Takahiro Nomoto, Hiroyasu Takemoto, Nobuhiro Nishiyama, Kanjiro Miyata,* Kazunori Kataoka*

For efficient delivery of siRNA into the cytoplasm, a smart block copolymer of poly(ethylene glycol) and charge-conversion polymer (PEG-CCP) is developed by introducing 2-propionic-3-methylmaleic (PMM) amide as an anionic protective group into side chains of an endosome-disrupting cationic polyaspartamide derivative. The PMM amide moiety is highly susceptible to acid hydrolysis, generating the parent cationic polyaspartamide derivative at endosomal acidic pH 5.5 more rapidly than a previously synthesized *cis*-aconitic (ACO) amide control. The PMM-based polymer is successfully integrated into a calcium phosphate (CaP) nanoparticle with siRNA, constructing PEGylated hybrid micelles (PMM micelles) having a sub-100 nm size at extracellular neutral pH 7.4. Ultimately, PMM micelles achieve the significantly higher gene silencing efficiency in cultured cancer cells, compared to ACO control micelles, probably due to the efficient endosomal escape of the PMM micelles. Thus, it is demonstrated that fine-tuning of acid-labile structures in CCP improves the delivery performance of siRNA-loaded nanocarriers.

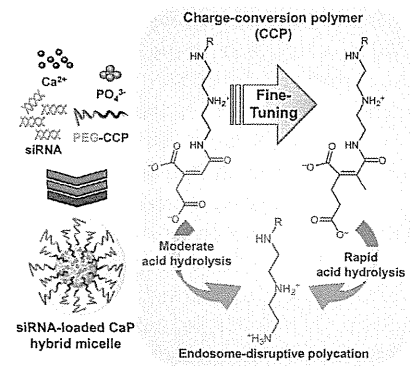

Y. Maeda, T. Nomoto, Prof. K. Kataoka
Department of Bioengineering, Graduate School of Engineering, The University of Tokyo, 7–3–1 Hongo, Bunkyo-ku, Tokyo 113–8656, Japan
E-mail: kataoka@bmw.t.u-tokyo.ac.jp
Dr. F. Pittella, Dr. K. Miyata, Prof. K. Kataoka
Center for Disease Biology and Integrative Medicine, Graduate School of Medicine, The University of Tokyo, 7–3–1 Hongo, Bunkyo-ku, Tokyo 113–0033, Japan
E-mail: miyata@bmw.t.u-tokyo.ac.jp
Dr. H. Takemoto, Prof. N. Nishiyama
Polymer Chemistry Division, Chemical Resources Laboratory, Tokyo Institute of Technology, R1–11, 4259 Nagatsuta, Midori-ku, Yokohama 226–8503, Japan
Prof. K. Kataoka
Department of Materials Engineering, Graduate School of Engineering, The University of Tokyo, 7–3–1 Hongo, Bunkyo-ku, Tokyo 113–8656, Japan

1. Introduction

Small interfering RNA (siRNA) has been greatly highlighted as a potential therapeutic agent for a variety of intractable diseases, including cancer.[1] To obtain therapeutic benefits, siRNA needs to be transported to the cytoplasm after cellular internalization. However, endocytosed macromolecules are generally entrapped by acidic vesicular compartments, i.e., endosomes, within cells, leading to the lysosomal degradation.[2] Hence, various polymeric materials have been developed to facilitate endosome disruption for smooth endosomal escape of siRNA.[3] Polyethylenimine (PEI) is one of the most widely used polymers for the endosomal escape of nucleic acids. It is believed that the low pK_a amines in PEI can serve as a proton sponge in acidic endosomes (pH ≈ 5.5) to

Macromol. Rapid Commun. **2014**, *35*, 1211–1215

DOI: 10.1002/marc.201400049

induce endosome disruption,[4,5] due to the increased osmotic pressure within the vesicles and/or the direct interactions of highly charged PEI with oppositely charged endosomal membrane.[6,7] However, significantly protonated PEI even under extracellular conditions (pH 7.4) concurrently induces the considerable cytotoxicity due to the cytoplasmic membrane damage.[8,9] Therefore, further development of endosome-disrupting polymers is still demanded for more efficient, yet less toxic endosomal escape of siRNA.

Our previous studies revealed that diaminoethane unit (—$NHCH_2CH_2NH$—) showed a distinctive change in the protonated state between pH 7.4 and 5.5, i.e., the monoprotonated state at pH 7.4 and the diprotonated state at pH 5.5.[10,11] Accordingly, a polyaspartamide derivative bearing the diaminoethane unit in the side chain, poly{*N*′-[*N*-(2-aminoethyl)-2-aminoethyl]aspartamide} (PAsp(DET)), successfully induced acidic pH-responsive membrane destabilization because of the change in its protonated state.[11–14] PAsp(DET) allowed efficient gene expression of plasmid DNA in cultured cells, associated with significantly lower cytotoxicity compared to PEI.[10–14] Meanwhile, primary amines in PAsp(DET) could be further modified with *cis*-aconitic (ACO) anhydride to generate an endosome-disrupting polyanion PAsp(DET-ACO), where ACO amide was subjected to acid hydrolysis for regeneration of the parent polycation PAsp(DET).[15] Thus, this polyanion was termed the charge-conversion polymer (CCP) based on its charge-conversion from the negative to the positive at acidic pH.

This CCP-based strategy was quite useful for siRNA delivery, when a block copolymer of poly(ethylene glycol) and CCP (PEG–CCP) was applied for construction of hybrid micelles with calcium phosphate (CaP) precipitates (Figure S1, Supporting Information).[16–18] CaP precipitates have been extensively used as a conventional transfection reagent of nucleic acids, because of their extremely low-cost and simple preparation scheme. However, the rapid growth of CaP crystal has substantially hampered the utilization of CaP precipitates for systemic nucleic acid delivery.[19] In this regard, PEG–CCP provided CaP precipitates with a PEG shell for size-controlling as well as biocompatibility to form monodispersive hybrid polymeric micelles. Indeed, siRNA-loaded hybrid micelles were prepared with CaP and PEG–CCP, having a size of sub-100 nm with a narrow size distribution, and induced efficient gene silencing in various cultured cancer cells.[16–18] Ultimately, systemically administered hybrid micelles showed the significant antitumor activity in a subcutaneous pancreatic cancer model by delivering the siRNA targeted for vascular endothelial growth factor.[17]

In our previous studies, the ACO amide, which is a maleic acid derivative bearing 2-acetic acid moiety, has been utilized as an acid-labile bond (Figure 1). It is known in this regard that the sensitivity of maleic acid amides to acid hydrolysis can be altered by functional groups substituted at the 2- and 3-positions of the maleic acid amide.[20] Indeed, 2-propionic-3-methyl maleic (PMM) amide was demonstrated to be more susceptible to acid hydrolysis compared to ACO amide.[21] This fact motivated us to finely tune the acid-labile amide structure in PEG–CCP for improving the endosome-escaping functionality. In the present study, a second generation of PEG–CCP was newly synthesized by introducing the PMM moieties into primary amines in PEG–PAsp(DET). The obtained block copolymer PEG–PAsp(DET-PMM) was compared with PEG-PAsp(DET-ACO) in terms of the sensitivity to acid hydrolysis and the delivery efficacy based on the hybrid micelle formulation.

2. Experimental Section

All experimental details are described in Supporting Information.

3. Results and Discussion

siRNA and its nanocarriers, once internalized into cells, are transported to the late endosomes (or the lysosomes),

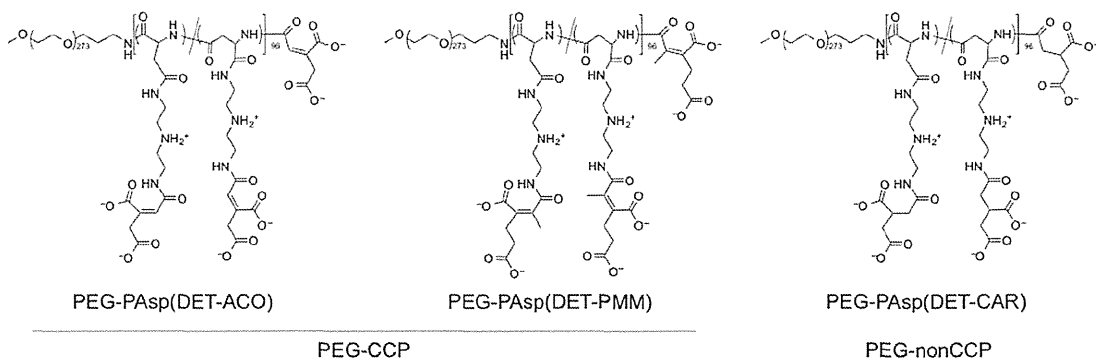

Figure 1. Chemical structures of PEG-PAsp(DET-ACO) and PEG-PAsp(DET-PMM) as PEG-CCPs, and PEG-PAsp(DET-CAR) as a PEG-nonCCP. The carballylic (CAR) moiety is a succinic acid derivative, and thus, its amide is much less sensitive to acid hydrolysis, compared to the maleic acid derivatives, PMM and ACO moieties.

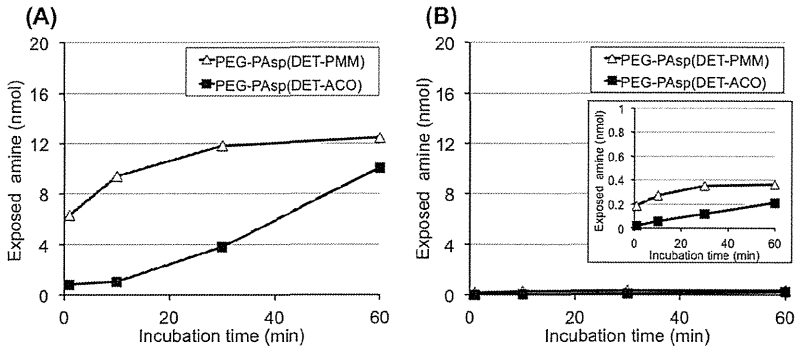

Figure 2. Amount of exposed amine in PEG–PAsp(DET–PMM) and PEG–PAsp(DET–ACO) after incubation at A) pH 5.5 and B) pH 7.4. The amount of exposed amine was determined from standard curves prepared with glycine solutions in an acetate buffer (pH 5.5) and a phosphate buffer (pH 7.4).

followed by lysosomal degradation.[2,22] Thus, they need to escape from those vesicular compartments to the cytoplasm before degrading for exerting gene silencing effect. Here, a smart block copolymer of biocompatible PEG and endosome-disrupting PAsp(DET–PMM) was synthesized by introducing a PMM moiety into primary amines in PAsp(DET) side chains through the amide bond formation (Figure 1 and Scheme S1, Supporting Information). It is reported that PMM amide is cleaved more rapidly than ACO amide in acidic conditions, probably because the pK_a value of carboxylates in dimethylmaleamylate derivatives is higher than that in citraconylate derivatives.[21] Thus, PAsp(DET–PMM) is expected to be more rapidly converted to the parent polycation PAsp(DET) in acidic endosomes compared with PAsp(DET–ACO), for facilitating the endosome disruption (Figure S1, Supporting Information). The successful synthesis of PEG–PAsp(DET–PMM) was confirmed from the size exclusion chromatogram (Figure S2, Supporting Information) and ^{1}H NMR spectrum (Figure S3 and Table S1, Supporting Information).

The charge-conversion functionality of PEG–PAsp(DET–PMM) was compared with that of PEG–PAsp(DET–ACO) by determining the amount of amines generated from the CCP segments at pH 7.4 and 5.5 (Figure 2). Obviously, PEG–PAsp(DET–PMM) exerted higher conversion rate than PEG–PAsp(DET–ACO) over time at both pHs of 5.5 and 7.4, demonstrating more rapid hydrolysis of the PMM amide bonds. Also, the accelerated hydrolysis at the lower pH of 5.5 was demonstrated for both CCP segments. Nevertheless, the considerable increase in the conversion ratios even at pH 7.4 is likely to induce destabilization of hybrid micelles under extracellular neutral conditions. Thus, the stability of hybrid micelles in serum-containing medium was further examined as described below.

The newly synthesized PEG–CCP, PEG–PAsp(DET–PMM), was applied for the preparation of CaP hybrid micelles loaded with siRNA and then characterized by DLS. The obtained DLS (volume-weighted) histogram of siRNA-loaded hybrid micelles prepared with PEG–PAsp(DET–PMM) (PMM micelles) displays a hydrodynamic diameter of ≈70 nm (Figure S4, Supporting Information), associated with a narrow size distribution (polydispersity index = 0.1), similar to hybrid micelles prepared with PEG–PAsp(DET–ACO) (ACO micelles). Note that the micelle formation was not observed in the absence of calcium and phosphate ions under the similar condition because of the hydrophilic nature of PEG–CCPs. In sharp contrast, non-PEGylated CaP precipitates showed much larger size (≈1 μm) (data not shown). These results demonstrate that the block copolymers with PEG were essential for the sub-100 nm nanoparticle formation due to enhanced colloidal stability based on the PEG shell.

The carrier stability under cell culture conditions is a prerequisite for efficient cellular uptake of siRNA. In our previous study, ACO micelles were confirmed to stably entrap siRNA in 10% fetal bovine serum (FBS)-containing Dulbecco's modified Eagle's medium (DMEM) for a relatively short incubation time of 4 h.[17] Nevertheless, the stable entrapment of siRNA in the micelles for longer incubation time (e.g., 24 h) is crucial from the standpoint of systemic delivery. Thus, the stability of hybrid micelles in the DMEM containing 10% FBS was investigated over 24 h at 37 °C by fluorescence correlation spectroscopy.[17,23] By assuming the spherical shape of hybrid micelles,[17,18] the obtained diffusion coefficients of hybrid micelles incorporating Alexa647-siLuc were converted to the corresponding hydrodynamic diameters based on the Stokes-Einstein equation (Figure S5, Supporting Information), and then, normalized to the value of naked siRNA. Both hybrid micelles maintained their initial size during 24 h incubation, indicating the stable encapsulation of siRNA within the hybrid micelles in the serum-containing medium. These results strongly suggest that PEG–PAsp(DET–PMM) and PEG–PAsp(DET–ACO) should be stably bound to CaP core without hydrolysis of maleic acid amides in the serum-containing medium at pH 7.4.

Next, the cellular internalization behavior of hybrid micelles was examined by a flow cytometer. Luciferase-expressing human ovarian cancer (SKOV3-Luc) cells were incubated with Cy5-siLuc-loaded hybrid micelles for 6 and 24 h, followed by the flow cytometric analysis (Figure 3A and Figure S6, Supporting Information). The significant cellular uptake of Cy5-siLuc was confirmed for all three hybrid micelles, i.e., PMM micelles, ACO micelles,